



## SCIANTIX: A new open source multi-scale code for fission gas behaviour modelling designed for nuclear fuel performance codes

D. Pizzocri , T. Barani , L. Luzzi \*

Politecnico di Milano, Department of Energy, Nuclear Engineering Division, Via La Masa 34, 20156, Milano, Italy



### HIGHLIGHTS

- The characteristics of the SCIAINTIX computer code are described.
- The models currently available in SCIAINTIX are detailed (with all the parameters).
- The verification of the numerical solvers is presented.
- Showcases of validation in both constant and transient conditions are presented.
- Future (short and long term) development plans are outlined.

### ARTICLE INFO

#### Article history:

Received 28 October 2019

Received in revised form

31 December 2019

Accepted 3 February 2020

Available online 6 February 2020

#### Keywords:

Multi-scale material modelling

Fission gas behaviour

Fuel performance code

Nuclear fuel

### ABSTRACT

Bridging lower length-scale calculations with the engineering-scale simulations of fuel performance codes requires the development of dedicated intermediate-scale codes. In this work, we present SCIAINTIX, an open source 0D stand-alone computer code designed to be included/coupled as a module in existing fuel performance codes. The models currently available in SCIAINTIX cover intra- and inter-granular inert gas behaviour in UO<sub>2</sub>, and high burnup structure formation as well. Showcases of validation in both constant and transient conditions are presented in this work. As for the numerical treatment of the model equations, SCIAINTIX is developed with full numerical consistency and entirely verified with the method of manufactured solutions – verification of different numerical solvers is also showcased in this work.

© 2020 The Authors. Published by Elsevier B.V. This is an open access article under the CC BY license (<http://creativecommons.org/licenses/by/4.0/>).

gas behaviour is a crucial aspect in fuel performance codes [1,3,8,12,13].

Two different approaches are possible to describe fission gas behaviour in the frame of fuel performance codes: (1) correlation-based approaches, in which fission gas release and gaseous swelling are calculated via expressions directly related to macroscopic variables of the fuel rod (e.g., fuel temperature and burnup) and tuned on experimental data [4,14–21], and (2) physics-based approaches, which aim at describing the physical mechanisms of fission gas behaviour within the fuel<sup>1</sup> [22–34]. These physics-based models often leverage kinetic rate theory [35,36] to describe the behaviour of fission gas atoms and their interaction with point and extended defects in the crystal [27,31].

### 1. Introduction

The predictive analysis of the behaviour of nuclear fuel rods under irradiation is one of the fundamental activities required for the safe design, licensing and operation of nuclear reactors [1–3]. For this purpose, fuel performance codes have been developed and validated [3–10]. These codes solve for the temperature, strain and stress fields in the fuel rod, considering the thermo-mechanical problem inherently coupled with the peculiar phenomena occurring in fuel and cladding as caused by irradiation [3]. Among these phenomena, fission gas behaviour – i.e., from an engineering point of view, fission gas release and gaseous swelling – is a potential life-limiting factor for the operation of nuclear fuel in light water and fast reactors [1,3,11,12]. For this reason, the modelling of fission

<sup>1</sup> Often hybrid approaches are used, combining correlation-based and physics-based models to describe different phenomena, e.g., a correlation can be used for fuel gaseous swelling and paired with a physics-based description of fission gas release as driven by diffusion (e.g., Refs. [4,17]), or representing only partial steps of the fission gas evolution through mechanistic approaches, relegating the remainder to empirical correlations [22].

\* Corresponding author.

E-mail address: [lelio.luzzi@polimi.it](mailto:lelio.luzzi@polimi.it) (L. Luzzi).

## Nomenclature

$A_{\text{gf}}$	Inter-granular bubble projected area	$\text{m}^2 \text{ bub}^{-1}$
$a$	Spherical grain radius	$\text{m}$
$a_m$	Limiting grain radius for grain-growth	$\text{m}$
$a_\infty$	Grain radius of recrystallized high burnup structure fuel	$\text{m}$
$bu$	Burnup	$\text{GWd t}_{0.02}^{-1}$
$bu_{\text{eff}}$	Effective burnup	$\text{GWd t}_{0.02}^{-1}$
$c_1$	Single-atom gas concentration	$\text{at m}^{-3}$
$D$	Intra-granular diffusion coefficient	$\text{m}^2 \text{ s}^{-1}$
$F$	Fission rate	$\text{fiss m}^{-3} \text{ s}^{-1}$
$F_{\text{gf}}$	Fractional coverage of grain faces	/
$F_{\text{gf,sat}}$	Saturation fractional coverage of grain faces	/
$f_{\text{gf}}$	Fraction of non-cracked grain faces	/
$g(bu)$	Function of burnup limiting grain-growth	—
$M$	Grain-boundary mobility	$\text{m}^2 \text{ s}^{-1}$
$m$	Gas concentration in intra-granular bubbles	$\text{at m}^{-3}$
$N_{\text{ig}}$	Intra-granular bubble concentration	$\text{bub m}^{-3}$
$N_{\text{gf}}$	Inter-granular bubble concentration	$\text{bub m}^{-2}$
$q$	Inter-granular gas concentration	$\text{at m}^{-3}$
$R_{\text{ig}}$	Intra-granular bubble radius	$\text{m bub}^{-1}$
$R_{\text{gf}}$	Inter-granular bubble radius	$\text{m bub}^{-1}$
$r$	Radial coordinate	$\text{m}$
$t$	Time	$\text{s}$
$y$	Fission gas yield	$\text{at fiss}^{-1}$
$\alpha$	Intra-granular re-solution rate	$\text{s}^{-1}$
$\beta$	Intra-granular trapping rate	$\text{s}^{-1}$
$(\Delta V/V)_{\text{ig}}$	Intra-granular swelling	/
$(\Delta V/V)_{\text{gf}}$	Inter-granular swelling	/
$v$	Intra-granular nucleation rate	$\text{bub m}^{-3} \text{ s}^{-1}$
$\tau$	Characteristic effective burnup for high burnup structure formation	$\text{GWd t}_{0.02}^{-1}$
$\Omega$	Gas atomic volume in the lattice	$\text{m}^3 \text{ at}^{-1}$

For the sake of brevity, at stands for atoms, fiss for fissions, bub for bubbles.

When engineering applications in fuel performance codes are targeted, physics-based models present potential limitations compared with correlation-based approaches. First, the numerical stability offered by the use of correlations is generally superior, bearing in mind that a fission gas release model is called at each time step, each mesh point, each convergence iteration of a fuel performance, i.e., a very high number of times [3,8]. Second, the computational effort required by physics-based model is generally higher than that required by correlation-based approaches [37]. Therefore, these aspects should be carefully considered when aiming at replacing correlation-based with physics-based models in fuel performance codes.

On the other hand, physics-based models offer inherent advantages compared to empirical correlations. First, since the phenomena to be described are governed by general evolution equations, they are applicable with minor modifications to different fuel materials [37–40]. Second, they are applicable for the simulation of either irradiation and annealing, and operational and transient conditions as well [22,24,31,34,41–43]. Third, physics-based models naturally benefit from the availability of novel experimental data, by extending their validation database, whereas correlation-based approaches require re-definition to incorporate new experimental data [37]. Lastly, physics-based models allow for exploiting the theoretical and experimental results from different scales<sup>2</sup> [31,44–51].

To leverage these advantages, different codes dealing with physics-based modelling of fission gas behaviour have been

developed [25,27,31–33,52–56]. These codes are either stand-alone or conceived to be used as fission gas behaviour modules within fuel performance codes (e.g., SIFGRS [57] for BISON [10,55], FISPRO2 [34,58] for TRANSURANUS [4,56], CARACAS [25] for ALCYONE [9,59], GRSW-A [32,60] for FALCON [7,61], and MFPR [31] for SFPR [62] and BERKUT [63]).

Recently, the investigation on fission gas behaviour basic mechanisms and the attempt to capitalize the results of this investigation in engineering scale simulations have been the subject of several international research initiatives [11,47,64–66].

The SCIANTIX code [67] presented in this paper is grafted into this research framework. It has been developed with a twofold objective:

- It aims at effectively bridging lower-length scale and engineering scale of fuel performance codes, feeding the latter with theoretical and experimental knowledge about fission gas behaviour mechanisms inferred by the former approaches. Thus, when possible, the use of physics-based models is preferred over correlation-based approaches, but always in line with the computational requirements of fuel performance codes.
- It aims at being usable as a stand-alone code for the simulation of separate effect experiments at the fuel-grain scale involving inert gas behaviour, both supporting the design of the experiment itself and the interpretation of the results.

In order to target these objectives, SCIANTIX has specific software features (Section 2) and embodies a consistent set of physics-based models (Section 3). Moreover, SCIANTIX is available as open source under MIT license [67], greatly easing its usage as fission gas behaviour module in existing fuel performance codes. Because of this licensing choice, all the models implemented in the currently available version of SCIANTIX are already published and validated. For this reason, after a summary of SCIANTIX validation we present

<sup>2</sup> While correlations are derived by fitting of experimental data, e.g. Refs. [16,18,21], physics-based models are derived from theoretical and experimental results, used to define both the structure of rate equations to be used and their parameters (e.g., diffusivities, solubilities, generation rates and so on). Moreover, physics-based model require validation both against separate-effect experiments (e.g., Refs. [26,31]) and against integral irradiation experiments [34,43] in order to be reliably applicable in fuel performance codes.

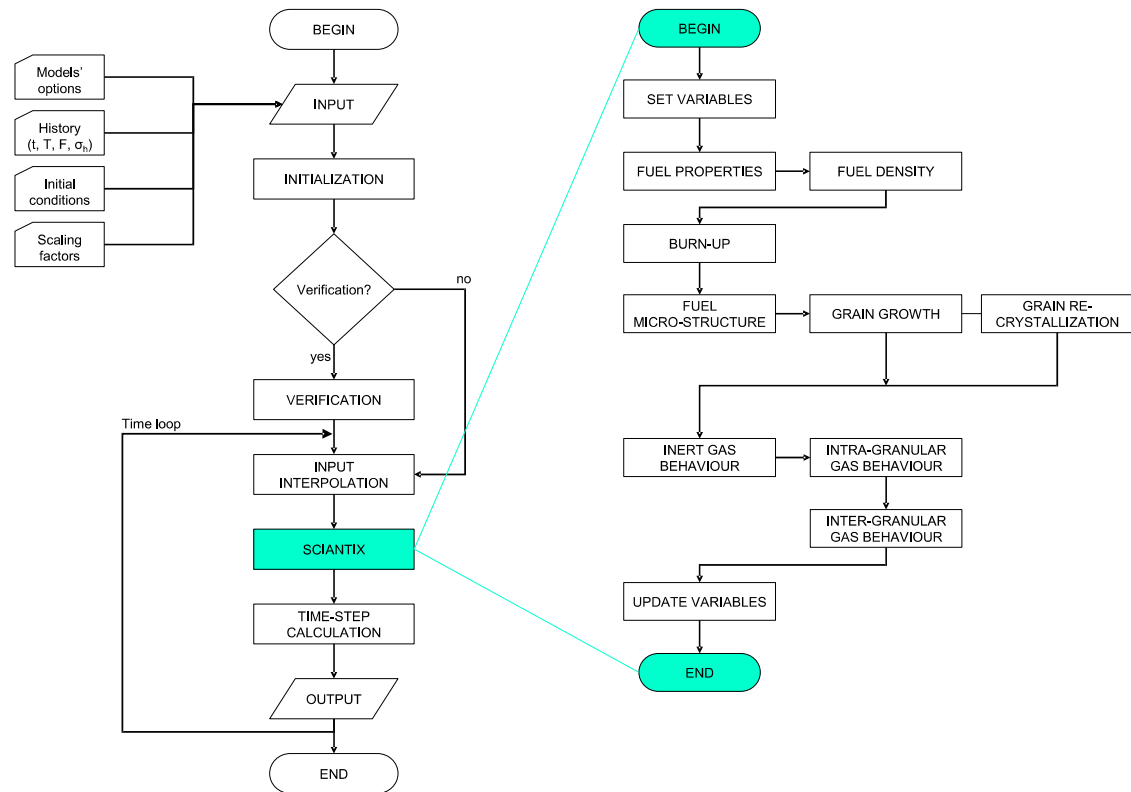


**Fig. 1.** Flow chart of SCIANTIX, highlighting the division between the external driver (parent code) and the meso-scale module. This flow chart is designed to ease inclusion of SCIANTIX in fuel performance codes.

a showcase of selected simulations detailing the behaviour of the main models (Section 4). Lastly, we provide an overview of the currently ongoing developments in SCIANTIX, which are going to be released open source as the results are published (Section 5).

## 2. Flow chart and numerical features

SCIANTIX is inherently designed as a module ready to be included/coupled with existing fuel performance codes (even in its stand-alone structure). For this reason, the flow chart reported in Fig. 1 is divided in two parts: (1) on the left, the external driver (referred to as parent code) and on the right (2) the SCIANTIX module itself. The parent code performs several fundamental operations, e.g., input reading, output printing, and time stepping. As shown in Fig. 1, beside model options, initial conditions of the state variables (i.e., quantities evolving continuously in time), and possible scaling factor for sensitivity/uncertainty purposes, the parent code performs the interpolation of the simulation history quantities (i.e., temperature, fission rate density, and hydrostatic stress) in the specified time intervals. In particular, the parent code linearly interpolates the history quantities between two consecutive time points, dividing the time step in a number of sub-timesteps, chosen *a priori*. In such sub-intervals, the SCIANTIX module performs the incremental calculation of the evolution of

physical state variables (e.g., grain radius, inert gas concentrations, gaseous swelling), updating the values of these variables in the parent code. This structure allows for straightforward coupling within fuel performance codes [8].

All the differential equations considered in the models implemented in SCIANTIX are solved with an implicit A-stable first order scheme, i.e., backward Euler.<sup>3</sup> All the numerical solutions are consistent, i.e., have the error decreasing proportionally with the decrease in time step. The numerical solvers are all collected in an independent part of the code and can be called for in the different models. This allows for a complete verification of the code through the verification – once and for all – of the numerical solvers and allows the developers of physical models to focus on the physics itself instead of on the numerical issues.<sup>4</sup> Table 1 reports all the solvers currently available in SCIANTIX.

Verification is performed via the method of manufactured solutions (MMS) [68]. Compared to other more arbitrary verification strategies (e.g., trend tests and comparisons evaluated by expert judgment [68]) MMS provides a more rigorous verification framework. The method of exact solutions (MES) is preferable to MMS if exact analytic solutions are available for the specific problem to be solved, which is not the case for the models available in SCIANTIX<sup>5</sup> and for many scientific codes as well. For these reason MMS is recommended for the verification of scientific software [68,69]. The steps required to apply MMS to verify a numerical solver are depicted in Fig. 2. SCIANTIX can perform the verification – selection

<sup>3</sup> It is worth noting that several models available in SCIANTIX are nonlinear, with the main source of non-linearity arising from the time-variation of the parameters. Dedicated approaches developed to handle this type of non-linearity are currently available, and applied in fuel performance codes especially for the solution of the fission gas diffusion equation [13,117,118]. These approaches are not applied in SCIANTIX, in order to preserve the consistency of all the numerical solutions in the code.

<sup>4</sup> This idea is not novel, e.g., the MOOSE platform developed by Idaho National Laboratory implements a very similar user-oriented approach [119].

<sup>5</sup> The analytic solution is generally well known for constant conditions, but time-varying situations occur in practically all the simulations.

**Table 1**

Enumeration of the solvers available in SCIANTIX and corresponding convergence order obtained through the MMS method.

Solver	General equation being solved	Order of convergence
Integrator	$dy/dx = S$	1
Decay	$dy/dx = -\lambda y + S$	1
Binary interaction	$dy/dx = -ky^2$	1
Limited growth	$dy/dx = -M/y + S$	1
Spectral diffusion	$dy/dx = D\nabla^2 y + S^a$	2
FORMAS	$dy/dx = D\nabla^2 y + S^a$	2

<sup>a</sup> This partial differential equation is solved for the spatial-average value of  $y$ .

block (diamond shaped) in the flow chart reported in Fig. 1 – of all the selected solvers prior to the simulation, producing dedicated verification outputs. The verification outcome for all the solvers is collected in Table 1.

Limited computational time is a fundamental requirement for a multi-scale module like SCIANTIX, which has the engineering goal of being used within fuel performance codes. In fact, when coupled with a fuel performance code, SCIANTIX represents a local (or point) model to be called at each mesh point, at each convergence iteration (since gaseous swelling and fission gas release feedback the thermomechanical behaviour of the fuel rod), and at each time step. Considering these considerable number of calls, SCIANTIX is designed to have a computational time in the order of milliseconds per call.<sup>6</sup> In order to ensure this limited computational time, all the models' differential equations are solved with an operator split approach,<sup>7</sup> i.e., sequenced based on their characteristic time constants and with coefficients evaluated at the beginning of time step.

### 3. Physics-based models

In this Section, we briefly describe the inert gas behaviour models for UO<sub>2</sub> available in the current version of SCIANTIX. More detailed information about each model can be found in dedicated publications [26,34,43,57,70,71].<sup>8</sup>

#### 3.1. Intra-granular fission gas behaviour

The description of intra-granular fission gas behaviour is typically the first and fundamental part of models for the prediction of fission gas release and swelling in nuclear fuel performance codes. The model currently available in SCIANTIX (described in detail in Ref. [26]) considers the fundamental processes of single gas atom diffusion, i.e., gas bubble nucleation, re-solution, and gas atom trapping at bubbles. The model is derived from a cluster dynamic formulation yet consisting of only three differential equations in its final form. It can hence be efficiently applied in engineering fuel performance codes while retaining a physical basis. The model equations are similar to state-of-the-art models currently used in fuel performance codes (see Ref. [72] for a complete review).

As for spatial problem, the intra-granular diffusion is treated

<sup>6</sup> It is worth noting that the stand-alone use of SCIANTIX requires in general a longer computational time compared to the use as a module in fuel performance codes, the difference being related to the file handling operations required to produce the output of SCIANTIX.

<sup>7</sup> The use of operator split approach is clearly a numerical approximation, required to ensure the computational performance of SCIANTIX. Depending on the simulation to be performed, this numerical approach may not be adequate, since it greatly simplifies the treatment of non-linearities (both in the state variables and in the coefficients). For this reason, an internal convergence loop is being developed and will be available in future versions as an alternative option.

<sup>8</sup> It is worth noting that all the models included in the open source version of SCIANTIX are already published. SCIANTIX is used for model development and testing on several other topics, from inert gas behaviour to actinide evolution, which are not yet available open source and therefore not detailed in this work.

with the classical Booth's approach [73], i.e., assuming a spherical grain of radius  $a$ . According to the approximation originally proposed by Speight [74], we solve for the total intra-granular gas concentration, given by the sum of the single-atom gas concentration  $c_1$  and the gas concentration trapped in intra-granular bubbles  $m$ <sup>9</sup>

$$\left\{ \begin{array}{l} \frac{\partial}{\partial t}(c_1 + m) = \frac{\alpha}{\alpha + \beta} D \frac{1}{r^2} \frac{\partial}{\partial r} r^2 \frac{\partial}{\partial r} (c_1 + m) + yF \\ \frac{d}{dt} N_{ig} = \nu - \alpha N_{ig} \end{array} \right. \quad (1)$$

where  $D$  is the single-atom diffusion coefficient (Table 2),  $\alpha$  is the re-solution rate (Table 3),  $\beta$  is the trapping rate (Table 4),  $y$  is the fission yield of fission gas,  $F$  is the fission rate,  $r$  is the radial coordinate within the grain and  $t$  is time. The term  $\alpha/(\alpha + \beta)D$  is referred to as the effective diffusion coefficient, accounting for the fraction of time single atoms are available for diffusion towards grain boundaries (i.e., not trapped in intra-granular bubbles).

As for the evolution of intra-granular bubble concentration  $N_{ig}$ , the current model assumes that bubbles are formed at a nucleation rate  $\nu$  (Table 5) and destroyed by irradiation induced re-solution<sup>10</sup>. The intra-granular bubble radius is then calculated assuming  $m/N_{ig}$  atoms in each bubble, i.e.,

$$R_{ig} = \left( \frac{3\Omega}{4\pi} \frac{m}{N_{ig}} \right)^{1/3} \quad (2)$$

where  $\Omega = 4.09 \text{ m}^3 \text{ at}^{-1}$  is the gas atomic volume in the lattice.<sup>11</sup> The intra-granular component of the gaseous swelling is derived

<sup>9</sup> The approximation proposed by Speight assumes that the trapping and re-solution of gas to and from intra-granular bubbles is faster than the diffusion towards the grain boundaries, therefore considering the evolution of the gas concentration in intra-granular bubbles as quasi-static. The limitations of this approach have been demonstrated theoretically by Veshchunov and Tarasov [24] through an alternative derivation of Eq. (1), and also shown non-adequate for particular fast transient conditions (timescales in the order of milliseconds, through numerical experiments [105]). Nevertheless, the approximation by Speight is practically effective in operational and relatively slow transient conditions (timescale in the order of seconds), and therefore still applied in fuel performance codes. For this reason, it is currently considered the default approach in SCIANTIX. Overcoming this quasi-static approximation is one of the envisaged developments of SCIANTIX.

<sup>10</sup> The intra-granular model currently does not consider the mobility of intra-granular bubbles in isothermal conditions. This mechanism has been observed experimentally at high temperatures (>1800 °C) [120] and confirmed by recent analysis [121] but the mechanism is still under investigation [122]. Straightforward extension of the model including this mechanism can be found in Ref. [58].

<sup>11</sup> This value, which is the volume of a Schottky trio (a neutral defect complex made by one uranium vacancy plus two oxygen vacancies) in the uranium dioxide lattice, is consistent with the measured (atomic) densities of intra-granular fission gas bubbles reported in Refs. [72,123,124]. It must be underlined that some atomic volumes occupied by Xe and Kr in intra-granular bubbles reported in the open literature (e.g. Ref. [125], based on Ronchi equation of state [126]) are derived considering equilibrium bubbles, yielding atomic volumes slightly higher than the ones reported in Refs. [72,123,124].

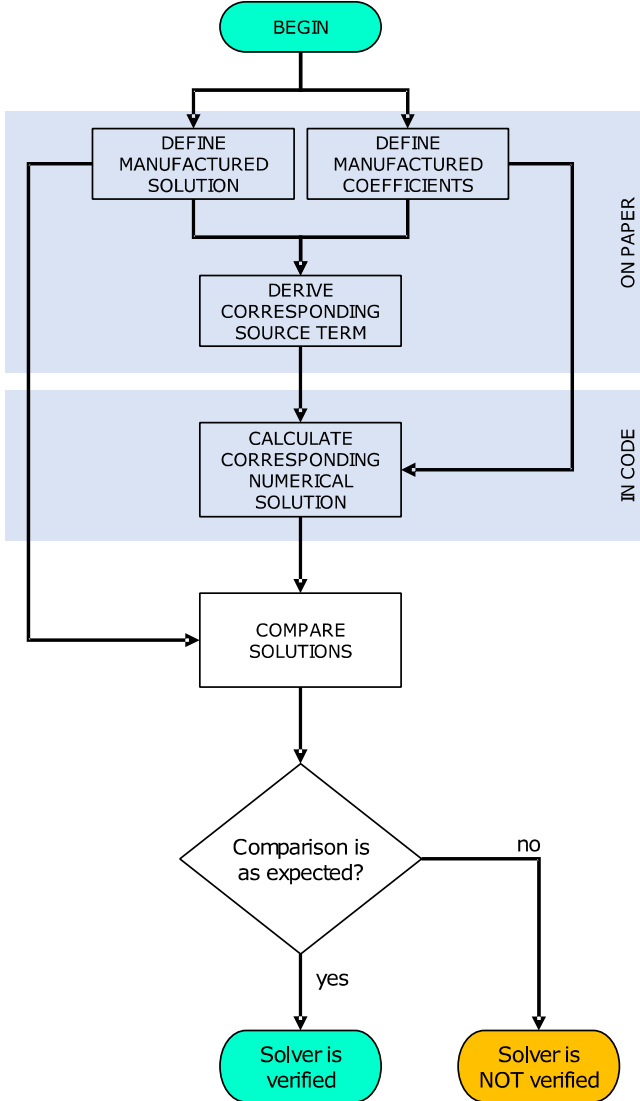


**Fig. 2.** Conceptual map of the method of manufactured solution (MMS) verification strategy [68]. This verification strategy is applied for every solver in SCIANTIX.

combining as

$$\left(\frac{\Delta V}{V}\right)_{ig} = \frac{4}{3} \pi N_{ig} R_{ig}^3 \quad (3)$$

### 3.2. Inter-granular inert gas behaviour

The inter-granular bubble evolution model adopted in SCIANTIX

**Table 2**

Options available for the fission gas diffusivity  $D$  ( $\text{m}^2 \text{s}^{-1}$ ).

Option	Correlation	Reference
0	$D = 0.0$	—
1	$D = D(T, F) = D_1 + D_2 + D_3$ $D_1 = 7.6 \cdot 10^{-10} \exp(-4.86 \cdot 10^{-19}/k_B T)$ $D_2 = 4.0 \cdot 1.41 \cdot 10^{-25} F^{1/2} \exp(-1.91 \cdot 10^{-19}/k_B T)$ $D_3 = 2.0 \cdot 10^{-40} F$ $F (\text{fiss m}^{-3} \text{s}^{-1})$ , fission rate $T (\text{K})$ , temperature $k_B (\text{J K}^{-1})$ , Boltzmann constant	[75]
2	$D = D(T) = 5.0 \cdot 10^{-8} \exp(-40,262/T)$	[13,76]

**Table 3**

Options available for the intra-granular re-solution rate  $\alpha$  ( $\text{s}^{-1}$ ).

Option	Correlation	Reference
0	$\alpha = 1.0 \cdot 10^{-4} \text{ s}^{-1}$	—
1	$\alpha = \alpha(R_{ig}, F) = 2\pi\mu_{ff}(R_{ig} + R_{ff})^2 F$ $\mu_{ff} = 6.0 \cdot 10^{-6} \text{ m}$ , fission fragment track length $R_{ff} = 1.0 \cdot 10^{-9} \text{ m}$ , fission fragment track radius $R_{ig}$ (m), intra-granular bubble radius $F (\text{fiss m}^{-3} \text{s}^{-1})$ , fission rate	[77]
2	$\alpha = \alpha(F) = 3.0 \cdot 10^{-23} F$	[29]

**Table 4**

Options available for the intra-granular trapping rate  $\beta$  ( $\text{s}^{-1}$ ).

Option	Correlation	Reference
0	$\beta = 1.0 \cdot 10^{-4} \text{ s}^{-1}$	—
1	$\beta = \beta(D, R_{ig}, N_{ig}) = 4\pi D(R_{ig} + R_{sg})N$ $R_{sg} = 0.2 \cdot 10^{-9} \text{ m}$ , xenon radius in the fuel lattice $D (\text{m}^2 \text{s}^{-1})$ , diffusion coefficient $R_{ig}$ (m), intra-granular bubble radius $N_{ig}$ (bub $\text{m}^{-3}$ ), intra-granular bubble density	[78]

**Table 5**

Options available for the intra-granular bubble nucleation rate  $\nu$  ( $\text{bub m}^{-3} \text{s}^{-1}$ ).

Option	Correlation	Reference
0	$\nu = 4.0 \cdot 10^{20} \text{ bub m}^{-3} \text{s}^{-1}$	—
1	$\nu = \nu(F) = 2\eta F$ $\eta = 25 \text{ bub ff}^{-1}$ $F (\text{fiss m}^{-3} \text{s}^{-1})$ , fission rate	[22,72,79]

is the one proposed by Pastore et al. [34,57], with the extension accounting for micro-cracking of grain boundaries in transient conditions [43,80]. This model is the default option in the BISON fuel performance code [10] and available in TRANSURANUS as well [4]. Remarkably, the model has been validated both as stand-alone against a set of separate effects experiments [81] in terms of inter-granular bubble swellings, and within TRANSURANUS against integral irradiation experiments in terms of integral fission gas release [34,43]. The model describes the evolution of the inter-granular gas concentration  $q$  as

$$\frac{\partial}{\partial t} q = - \left[ \frac{3}{a} \frac{\alpha}{\alpha + \beta} D \frac{\partial}{\partial r} (c_1 + m) \right]_{r=a} - R \quad (4)$$

The source term for  $q$  is the flux of single atoms diffusing from inside the fuel grain, whereas the release term  $R$  is modelled accounting for different phenomena:

1. Gas atoms arriving at the grain boundaries are collected in inter-granular bubbles, which are assumed to be one-off nucleated (e.g., Ref. [30]) on grain faces. No single atoms are assumed to exist at grain boundaries, since it is assumed that the trapping of single gas atoms is faster than the other processes<sup>12</sup> and re-

<sup>12</sup> These modelling assumption (one-off nucleation and instantaneous trapping) do not allow for the description of phenomena such as circulation, in which single gas atoms undergo to a re-solution from inter-granular bubbles back into the matrix, hence constituting an additional source term for the flux of gas atoms possibly transported to the grain edges. This phenomenon, which is considered e.g. in the MFPR code [31], requires the description of irradiation-induced re-solution of gas atom from inter-granular bubbles (e.g., Ref. [127]), plus the modeling of grain-edges gas bubbles. In the model employed in SCIANTIX, based on Pastore et al. [34], these two features are not included, thus gas circulation at grain boundaries cannot be modelled.

**Table 6**Options available for the inter-granular vacancy diffusion coefficient  $D_v$  ( $\text{m}^2 \text{s}^{-1}$ ).

Option	Correlation	Reference
0	$D_v = 1.0 \cdot 10^{-30} \text{ m}^2 \text{s}^{-1}$	—
1	$D_v = 6.9 \cdot 10^{-4} \exp(-3.88 \cdot 10^4/T)$ $T(\text{K}), \text{temperature}$	[88]
2	$D_v = (3/5) \cdot 8.86 \cdot 10^{-6} \exp(-4.17 \cdot 10^4/T)$	[57]

solution of gas from inter-granular bubbles is neglected. Moreover, grain-edges bubbles are not modelled.

2. Inter-granular bubbles, assumed of lenticular shape with circular projection on grain faces, are pressurized by gas atoms and grow by diffusion-controlled – with vacancy diffusivity at the grain boundaries  $D_v$  – vacancy absorption towards an equilibrium pressure [82] (Table 6).
3. The bubbles interconnect because of their growth. The inter-granular bubble concentration  $N_{\text{gb}}$  ( $\text{bub m}^{-2}$ ) on grain faces decreases as their projected area on the grain face  $A_{\text{gf}}$  ( $\text{m}^2 \text{bub}^{-1}$ ) grows following  $dN_{\text{gf}}/dA_{\text{gf}} = -2N_{\text{gf}}^2$  [30].
4. The net result of inter-granular bubble growth and interconnection is the increase of the grain-face fractional coverage  $F_{\text{gf}} = N_{\text{gf}} A_{\text{gf}} / (.)$ . When the fractional coverage reaches a saturation value  $F_{\text{gf}} = F_{\text{gf,sat}} = 0.5$ , it is assumed that a percolated path along the grain faces is formed, allowing for the release of gas from the grain boundaries.
5. The swelling rate decreases as the percolation of grain boundaries occurs, since the gas atoms diffusing from the interior of the grains are not entirely stored in the grain-boundary bubbles once percolation occurred.

The inter-granular swelling is mechanistically described according to

$$\left(\frac{\Delta V}{V}\right)_{\text{gf}} = \frac{3}{a} \frac{4\pi}{3} N_{\text{gf}} R_{\text{gf}}^3 \quad (5)$$

where  $R_{\text{gf}}$  ( $\text{m bub}^{-1}$ ) is the radius of inter-granular bubbles and  $3/a$  is the surface-to-volume ratio of fuel grains.

On top of this model describing the evolution of grain-face bubbles fed by intra-granular diffusion and allowing for fission gas release, we consider a semi-empirical description of a mechanism of grain-boundary micro-cracking [11,83–86], based on [43,80]. By introducing the fraction of non-cracked grain-faces  $f_{\text{gf}}$ , we can write its influence on the fractional coverage  $F_{\text{gf}}$  and the saturation fractional coverage of grain boundaries  $F_{\text{gf,sat}}$  as

$$\begin{aligned} \frac{dF_{\text{gf}}}{dt} &= \frac{\partial F_{\text{gf}}}{\partial q} \frac{dq}{dt} + F_{\text{gf}} \left( \frac{df_{\text{gf}}}{dt} \right) \\ \frac{df_{\text{gf,sat}}}{dt} &= F_{\text{gf,sat}} \left( \frac{df_{\text{gf}}}{dt} \right) \end{aligned} \quad (6)$$

where the evolution of the fractional coverage is described as the super-position of the inflow of gas atoms (and the consequent grain-boundary bubble evolution) and the micro-cracking of grain boundaries. The evolution of  $f_{\text{gf}}$  is described by an empirical micro-cracking parameter, which is a function of temperature and burnup, accounting for micro-cracking during heating and cooling transients [83–86] and healing of micro-cracks with burnup [87].

### 3.3. Micro-structure evolution

The grain growth process is strictly related to fission gas

behaviour [1,12] and therefore its treatment is required in SCANTIX. Grain growth has two major consequences: (1) it affects the diffusion rate towards the grain boundaries,  $D/a$ ,<sup>2</sup> and (2) while moving during the grain growth process, grain boundaries effectively sweep the fuel, collecting gas and gas bubble as a net at a rate  $3a^2(d\alpha/dt)$  [89–91]. The model currently available in SCANTIX is based on the work of [92,93], drawn on the formulation of Hillert [94] and accounting for the so-called Zener pinning effect [95], reading

$$\frac{da}{dt} = 4M \left( \frac{1}{a} - \frac{g(bu)}{a_m} \right) \quad (7)$$

where  $M = 1.46 \cdot 10^{-10} \exp(-32,114.5/T)^{13}$  is the grain-boundary mobility,  $g(bu) = 1 + 0.002 bu$  is an empirical function of burnup  $bu$ , and  $a_m = 2.23 \cdot 10^{-3} \exp(-7620/T)$  is the limiting grain size for a given temperature  $T$ .

Besides the normal grain growth process, relevant for low burnups (e.g., Refs. [95–97]), also the formation of high burnup structure involves a recrystallization of grains, *de facto* changing the grain size [98–100]. The description of the formation and evolution of high burnup structure is herein described as just affecting the (average) grain size.<sup>14</sup> The model describing high burnup structure formation and depletion currently available in SCANTIX is based on the concept of effective burnup, i.e., the burnup integrated below a certain temperature threshold (e.g., Refs. [32,101]), as representative of the accumulation of radiation damage triggering recrystallization. Namely, the evolution of the “average” grain size<sup>15</sup> is described by

$$\frac{da}{dbu_{\text{eff}}} = -\frac{1}{\tau} (a - a_\infty) \quad (8)$$

where,  $bu_{\text{eff}}$  is the effective burnup, i.e., the burnup integrated below 1000 °C,  $\tau = 5 \text{ GWD t}_{\text{UO}_2}^{-1}$  is the characteristic burnup governing the high burnup structure formation rate, and  $a_\infty = 150 \cdot 10^{-9} \text{ m}$  is the grain radius of recrystallized grains in the high burnup structure of UO<sub>2</sub> (e.g., Refs. [98,99]).

## 4. Showcase of results

Stand-alone validation of the physics-based models available in SCANTIX has been performed for each of the described models and is extensively reported in previous publications [26,34,70]. Together with the comparison with experimental data, the referenced publications include also comparison between the results of the models currently available in SCANTIX and those of several

<sup>13</sup> The mobility of grain boundaries herein reported is based on the experimental data of [95]. It is possible to apply the model for grain growth available in SCANTIX with other correlations for grain-boundary mobility derived from lower-length scale analysis [128–131] or from another experimental dataset (e.g., Refs. [96,132]). The grain-boundary mobility may be defined accordingly to the exponent of  $a$  on the right-hand side of Eq. (7), (1) in the current formulation), but different exponents may be found in the literature ([94,133]).

<sup>14</sup> The formation of high burnup structure strongly affects fission gas behaviour in the interested regions of the fuel [12,99,134]. A comprehensive description of the gas behaviour in high burnup structure is currently under development in SCANTIX [135], with several physics-based model already available in the open literature [31,32,39,40,136–140].

<sup>15</sup> The formation of high burnup structure may be depicted as a phase transition, with one phase being the unstructured fuel, and the other phase being the recrystallized fuel (e.g., see the modelling approach in Refs. [32,141]). The herein proposed description averages out these two phases by defining an average phase featured by a representative grain size, evolving from the unstructured value to the recrystallized value. The model is being developed overcoming this simplification and will be available in SCANTIX in the near future [135].

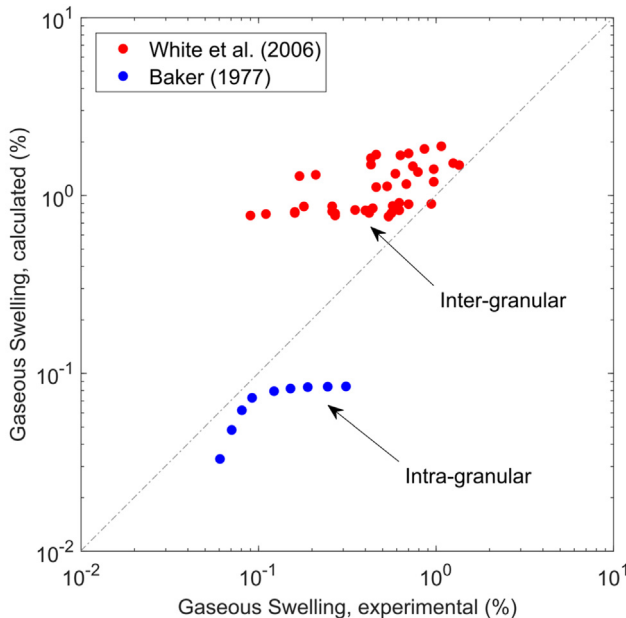


**Fig. 3.** Comparison of calculated intra- and inter-granular gaseous swelling by SCIAINTIX to experimental data by Baker [79] (swelling due to intra-granular bubbles, blue markers) and by White and co-workers [81] (swelling due to inter-granular bubbles, red markers). (For interpretation of the references to colour in this figure legend, the reader is referred to the Web version of this article.)

state-of-the-art models available in the open literature. Moreover, the validation strategy applied for SCIAINTIX involves the comparison between integral irradiation experiments results and the simulation results of fuel performance codes including SCIAINTIX as fission gas behaviour module. Also, these comparisons have been published in dedicated publications<sup>16</sup> [43,80,102]. For the sake of completeness, we report a summary of the validation database of SCIAINTIX, comparing the calculations to experimental results in terms of gaseous swelling. These results are complemented by a detailed showcase of selected SCIAINTIX simulations (still compared with experimental results) in relevant cases (both constant and transient conditions). Finally, we apply the SCIAINTIX code to the simulation of an irradiation history typical of a reactivity initiated accident (RIA) scenario, to showcase the capabilities of the code in accident conditions.

#### 4.1. Gaseous swelling results from the overall SCIAINTIX validation database

Stand-alone validation of SCIAINTIX against experimental data in terms of gaseous swelling is presented in Fig. 3. In this Figure, we compare the predictions on both intra-granular swelling (i.e., swelling due to intra-granular bubbles as defined by Eq. (3)) and inter-granular swelling (i.e., swelling due to grain boundary bubbles, as defined by Eq. (5)).

The experimental database by Baker [79] includes irradiation at constant temperatures (from 1273 K to 2073 K) and low burn-up ( $6.5 \text{ GWd t}_{\text{UO}_2}^{-1}$ ) of standard uranium dioxide fuels in the UKAEA's Winfirth SGHWR. The comparison to experimental data is reported in Fig. 3 (blue markers) and the values are collected in Table 7. The results are in line with those ones shown in a previous

**Table 7**

Comparison of calculated intra-granular gaseous swelling to experimental data for the analysed fuel samples from Baker [79].

Test Temperature (K)	Experimental (%)	Calculated (%)
1273	0.06	0.033
1373	0.07	0.048
1473	0.08	0.062
1573	0.09	0.073
1673	0.12	0.079
1773	0.15	0.082
1873	0.18	0.083
1973	0.24	0.084
2073	0.31	0.086

publication of the intra-granular model employed in SCIAINTIX [26], and demonstrate an acceptable deviation from the experimental data in terms of gaseous swelling. For a more thorough analysis of this experimental database, we refer the reader to Ref. [26].

Comparison of the predicted gaseous swelling due to inter-granular bubbles to experimental data is also included in Fig. 3. The experimental cases are taken from the database by White and co-workers [81]. The database consists in measurements performed on uranium dioxide Advanced Gas Reactor samples of fuel rods irradiated up to burnup between 9 and 21 GWd/t<sub>UO<sub>2</sub></sub> in the Halden reactor. After the base irradiation, rods were subjected to power ramp or power cycle histories.

The comparison shows a satisfactory agreement between calculated and measured data (collected in Table 8) yet demonstrating an overestimation of the low swelling data. Indeed, the results obtained through SCIAINTIX are in-line with a previous publication entailing the same model for inter-granular bubble evolution and experimental database [34].

#### 4.2. Constant conditions

To showcase detailed SCIAINTIX results in constant conditions, we selected the simulation of one of the experimental fuel samples by Baker [79] and summarized in Section 4.1. The sample has been analysed using transmission electron microscopy to measure intra-granular bubble concentration and intra-granular bubble radius.

The simulation in SCIAINTIX is set up with an irradiation history of 5,500 h with a constant fission rate of  $1 \cdot 10^{19} \text{ fiss m}^{-3} \text{ s}^{-1}$  (resulting in  $\approx 2 \cdot 10^{26} \text{ fiss m}^{-3} \approx 6.5 \text{ GWd t}_{\text{UO}_2}^{-1}$ ), at a constant temperature of 1300 K and with no hydrostatic stress. The default model parameters required in Eqs. (1)–(3) are used (i.e., option 1 in Tables 2–6), namely Turnbull's diffusivity [75], heterogeneous nucleation [22,72,77], Turnbull's heterogeneous re-solution rate [22], and diffusional trapping [78].

Fig. 4 reports the evolution of intra-granular bubble concentration and of intra-granular bubble radius as a function of burnup as simulated by SCIAINTIX, compared with the experimental results available at end of irradiation [79]. First, the agreement between simulated and experimental results is satisfactory. The agreement with experiments is particularly good for the intra-granular bubble radius, which is dominant compared to the intra-granular bubble concentration in determining the intra-granular swelling (third power in Eq. (3)). Besides the values at the end of irradiation, it is interesting to discuss the evolution of the variables along burnup. The intra-granular bubble concentration evolves according to Eq. (1). Due to the selection of a heterogeneous nucleation rate and a heterogeneous re-solution rate as model parameters, after an initial increase due to nucleation, the evolution of the intra-granular bubble concentration is asymptotically determined by the ratio of these two parameters, i.e., when  $dN_{\text{ig}}/dt \rightarrow 0$ , then  $N_{\text{ig}} \rightarrow \nu/\alpha = \eta/[2\pi\mu_{\text{ff}}(R_{\text{ig}} + R_{\text{ff}})^2]$ . The only variable in the right-hand side is the

<sup>16</sup> In several of the cited references, SCIAINTIX is not explicitly mentioned. In Refs. [26,70] SCIAINTIX has been indeed applied. On the other hand, in Refs. [43,80,102] different software implementations of the models have been used.

**Table 8**

Comparison of calculated inter-granular gaseous swelling to experimental data for the analysed fuel samples from White and co-workers [81].

Sample ID	SEM zone ID	Experimental (%)	Calculated (%)
4000	1	0.97	1.19
4000	2	0.68	1.16
4000	3	0.53	1.13
4000	4	0.46	1.12
4000	5	0.17	1.29
4004	1	0.62	0.91
4004	2	0.7	0.89
4004	3	0.44	0.85
4004	4	0.56	0.79
4004	5	0.27	0.77
4004	6	0.16	0.81
4005	1	0.94	0.89
4005	2	0.57	0.87
4005	3	0.42	0.82
4005	4	0.54	0.76
4005	5	0.27	0.79
4064	1	1.07	1.89
4064	2	0.86	1.83
4064	3	0.63	1.68
4064	4	0.74	1.46
4064	5	0.59	1.33
4065	1	1.25	1.52
4065	2	1.35	1.48
4065	3	0.97	1.41
4065	4	0.79	1.35
4065	5	0.21	1.31
4135	1	0.42	0.79
4135	2	0.16	0.79
4135	3	0.09	0.77
4136	1	0.6	0.83
4136	2	0.62	0.83
4136	3	0.26	0.81
4136	4	0.11	0.79
4140	1	0.26	0.87
4140	2	0.18	0.86
4162	1	0.7	1.72
4162	2	0.46	1.69
4162	3	0.43	1.62
4162	4	0.43	1.49
4163	1	0.6	0.85
4163	2	0.59	0.84
4163	3	0.35	0.83
4163	4	0.4	0.82

intra-granular bubble radius  $R_{ig}$ , therefore as the intra-granular bubble radius increases steadily as a result of trapping, the bubble concentration decreases with burnup.

As for the growth of the radius of intra-granular bubbles, it is governed by Eq. (2), in particular by the ratio between the intra-granular gas concentration trapped in bubbles and the bubble concentration, i.e.,  $m/N_{ig}$ . The intra-granular gas concentration in bubbles is depicted in Fig. 5, together with the evolution of the other gas concentrations. The gas evolution is governed by Eqs. (1), (4). The gas produced increases linearly as  $yF$ . A fraction of it, the intra-granular gas concentration,  $c_{1+m}$ , remains inside the grain after the diffusion process occurs. The gas that reaches the grain boundary,  $q$ , is eventually released when the saturation of grain boundaries is reached (see the change of slope in the curve in Fig. 5). The release process occurring in this irradiation history is purely diffusion-based, since no temperature variations. According to the model described in Section 3.2, the gas release occurs only after the saturation of grain boundary is reached (in line with the change of slope in the inter-granular gas concentration).

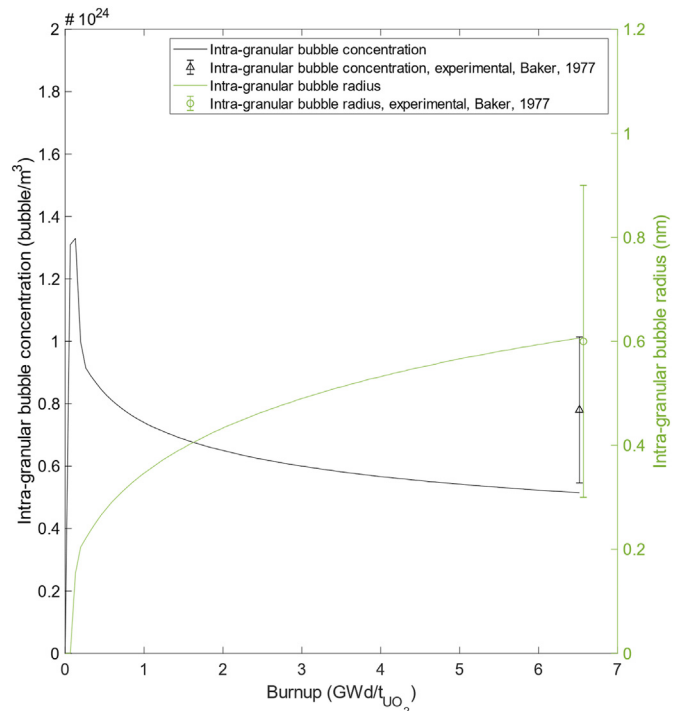


**Fig. 4.** Evolution of intra-granular bubble concentration and intra-granular bubble radius as a function of burnup in constant conditions ( $1373 \text{ K}, 1 10^{19} \text{ fiss m}^{-3} \text{ s}^{-1}$ ) as predicted by SCIANTIX, compared with the experimental results by Baker [79].

The behaviour of gas at the grain boundaries is clear from Fig. 6. The inter-granular bubble concentration  $N_{gf}$  decreases from the initial value  $4 10^{13} \text{ bub m}^{-3}$  (model parameter representing a one-off nucleation [30,34]) as the bubble size  $A_{gf}$  increases due to the inflow of gas from inside the grains and the absorption of vacancies due to bubble over pressurization. As bubble growth and interconnection proceeds, the fractional coverage  $F_{gf} = N_{gf}A_{gf}$  increases steadily, up to the saturation value  $F_{gf} = F_{gf,sat} = 0.5$ . The instant at which the saturation is reached corresponds to onset of fission gas release in Fig. 5.

#### 4.3. Transient conditions

To showcase the application of SCIANTIX in transient condition we selected an irradiation case among those analysed by White and co-workers [81] and presented in Section 4.1. This case study allows to discuss in more detail the behaviour of the grain-boundary model. The considered fuel sample (referred to as 4000C§A), after a base irradiation at low temperature ( $<900^\circ\text{C}$ ) up to a local burnup of  $17.5 \text{ GWd t}_{\text{UO}_2}^{-1}$  (corresponding to an irradiation of  $35,600 \text{ h}$  at a constant fission rate of  $4.15 10^{18} \text{ fiss m}^{-3} \text{ s}^{-1}$  and a constant hydrostatic stress of  $-0.21 \text{ MPa}$ , based on ENIGMA [54] calculations [81]), has been subject to a ramp test characterized by (1) a conditioning step of  $288 \text{ h}$  at  $884^\circ\text{C}$ ,  $4.15 10^{18} \text{ fiss m}^{-3} \text{ s}^{-1}$ , and  $-0.21 \text{ MPa}$ , followed by (2) a ramp up of  $1.52 \text{ min}$  up to (3) a holding of  $30 \text{ min}$  at  $1775^\circ\text{C}$ ,  $1.08 10^{19} \text{ fiss m}^{-3} \text{ s}^{-1}$ , and  $-14.8 \text{ MPa}$ , followed by (4) a ramp down of  $100 \text{ s}$  down to (5) a final holding of  $99 \text{ min}$  at  $884^\circ\text{C}$ ,  $4.15 10^{18} \text{ fiss m}^{-3} \text{ s}^{-1}$ , and  $-0.21 \text{ MPa}$ , and (6) a fast SCRAM (Fig. 7).

Fig. 8 reports the evolution of gas concentration as a function of temperature, as predicted by SCIANTIX. In this representation, the base irradiation and the conditioning step are vertical lines at  $1157 \text{ K}$ , while the holding on the of the ramp is the vertical line at  $2048 \text{ K}$ . Each line can be followed by the beginning of the ramp test

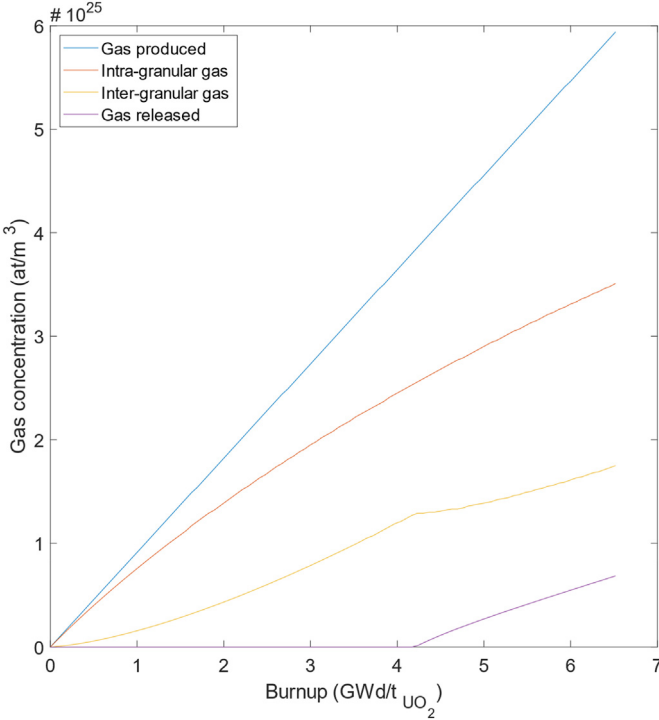


**Fig. 5.** Evolution of gas concentrations a function of burnup in an irradiation history [79] with constant conditions ( $1373\text{ K}, 1\text{ }10^{19}\text{ fiss m}^{-3}\text{ s}^{-1}$ ) as predicted by SCIANTIX.

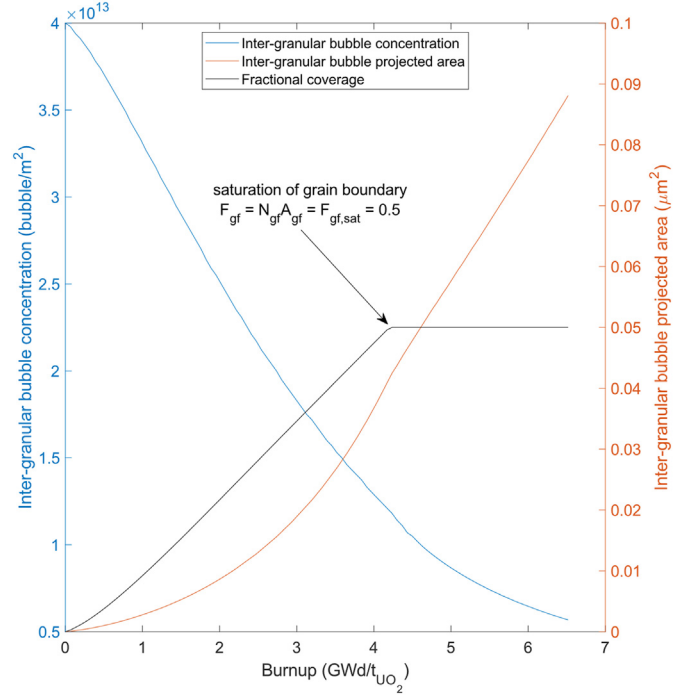


**Fig. 6.** Evolution of inter-granular bubble concentration, projected area, and fractional coverage as a function of burnup in an irradiation history [79] with constant conditions ( $1373\text{ K}, 1\text{ }10^{19}\text{ fiss m}^{-3}\text{ s}^{-1}$ ) as predicted by SCIANTIX.

(BRT) towards the end of the ramp test (ERT). Moving right along a line corresponds to a temperature increase, moving vertically to a step at constant temperature, and moving left to a temperature decrease.

The first observation from Fig. 8 is that the produced gas is practically constant. Second, during this ramp test the intra-granular gas concentration (almost) never grows, besides the temperature and consequently diffusivity increases. This is caused by the competition of intra-granular bubble trapping and diffusion towards the grain boundaries. It can be seen from Fig. 8 that the gas is transferred from intra-granular solution to intra-granular bubbles during the heating and the holding, and back from intra-granular bubbles to the solution during the cooling period, with a net trapping effect visible at ERT.

As for the gas at the grain boundaries, it is clear from Fig. 8 that it is released during the heating, the holding at high temperature, and the cool down as well. During the heat up, the release is mainly caused by the micro-cracking of grain boundaries and partially by the diffusional release following grain-boundary bubble coalescence (as discussed, no additional gas arrives at the grain boundary during the ramp test, but the increase in temperature causes an increase in bubble pressure, triggering bubble growth by vacancy absorption).

The contributions to fission gas release arising from either micro-cracking of grain boundaries or diffusional release can be isolated by looking at the evolution of the grain-boundary coverage as a function of temperature (Fig. 9a). From the base irradiation of 1157 K, the grain-face fractional coverage slightly increases during the first moments of the heat up step (up to  $\approx 1800$  K), reaching the saturation value and therefore triggering diffusional release. Above 1800 K it then steadily decreases due to the micro-cracking of grain faces during temperature transients and remains constant (at the saturation value) during the holding at 2048 K. Fig. 9b depicts the

evolution of grain-boundary swelling and of fractional fission gas release as a function of temperature, which are directly related to the evolution of fractional coverage, the main difference being the increase of grain-boundary swelling during the high temperature holding because of vacancy absorption. It is evident that the onset of fission gas release as the fractional coverage reaches the saturation value. Lastly, Fig. 9b reports the satisfactory agreement of the grain-boundary swelling predicted by SCIANTIX with the experimentally measured value.

#### 4.4. Accident conditions

As a last showcasing of SCIANTIX capabilities, we present the simulation of a representative RIA transient scenario. It is clear that the scope of this section is not to demonstrate the capability of SCIANTIX of performing a safety analysis, which would be impossible with a 0D stand-alone code, but only to provide an example of SCIANTIX performance during a very fast (accidental) transient.

As an exemplificative RIA case we select the CABRI REP-Na5 power pulse experiment [103]. This experiment involved a Gaussian-type power pulse of 8.8 ms full width at half maximum injecting  $451\text{ J g}^{-1}$  in a UO<sub>2</sub>/Zr-4 rodlet previously irradiated to 64 GWd t<sub>HM</sub><sup>-1</sup>. The analysis herein reported considers a point within the fuel pellet close to the pellet periphery. The evolution of the radial temperature profile during the transient test was derived in Ref. [103] by SCANAIR-3.2 calculations. The input conditions for the SCIANTIX simulation,<sup>17</sup> i.e., temperature and fission rate evolution as a function of time – reported in Fig. 10, are directly extracted from the results presented in Ref. [103].

<sup>17</sup> A base irradiation in constant conditions ( $900\text{ K}, 1\text{ }10^{19}\text{ fiss m}^{-3}\text{ s}^{-1}$ ) up to the burnup prior to the transient test has been postulated.

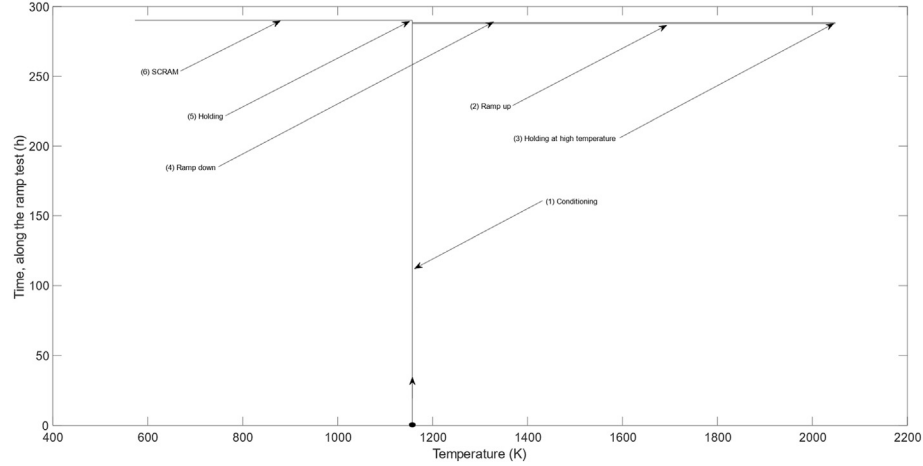


**Fig. 7.** Temperature history for the sample 4000C\$A from White et al. [81]. The (unusual) choice of plotting time as a function of temperature has the scope of easing the reading of Figs. 8 and 9. Temperature is a more natural variable for this transient, and it allows a clearer description of the model behaviour compared to time (due to the brevity of the ramp compared to the conditioning period).

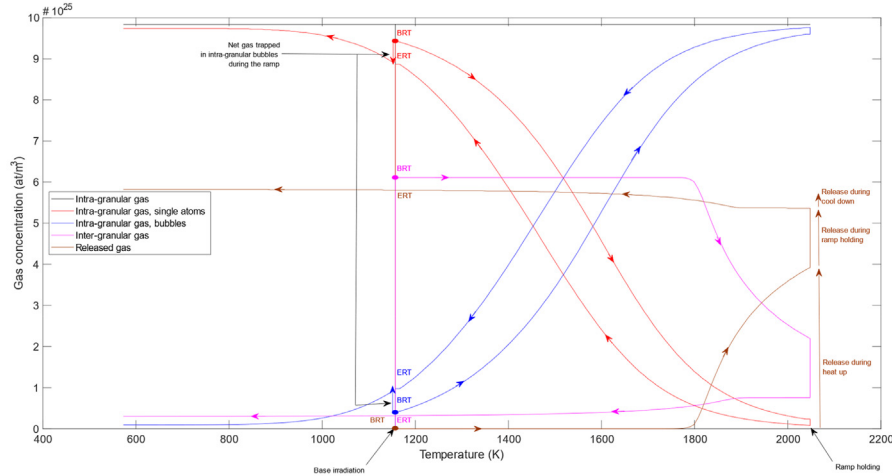


**Fig. 8.** Evolution of the gas concentrations as a function of temperature, simulated by SCIAINTIX for the sample 4000C\$A from White et al. [81]. From the beginning of the ramp test (BRT), moving right corresponds to a heating transient, vertical lines correspond to temperature holdings, and moving left correspond to a cooling transient. The end of the ramp is marked by ERT.

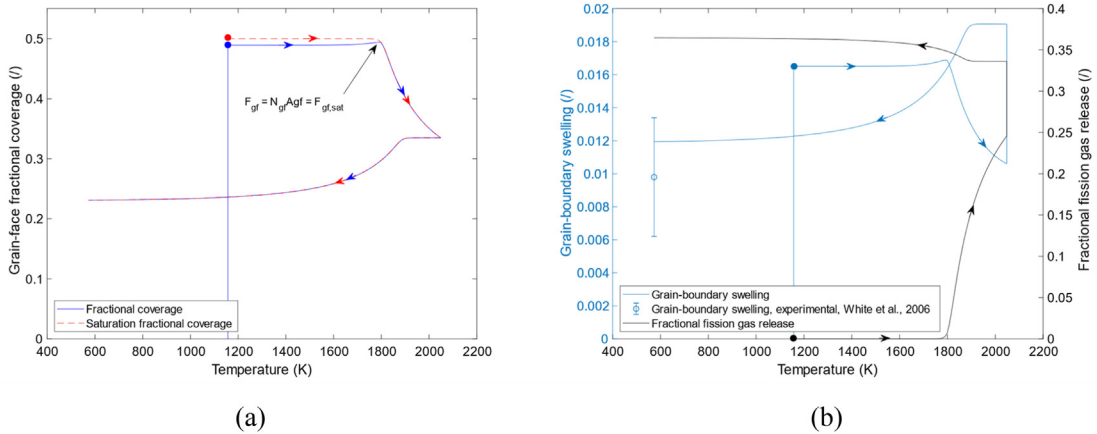


**Fig. 9.** Evolution of (a) the grain-face fractional coverage, saturation fractional coverage (dashed line), and (b) grain-boundary swelling and fractional fission gas release as a function of temperature, simulated by SCIAINTIX for the sample 4000C\$A by White et al. [81]. Base irradiation corresponds to the vertical line at 1157 K, moving right corresponds to a heating transient, the holding on top of the power/temperature ramp corresponds to the vertical line at 2048 K, and moving left corresponds to the cooling transient, down to 573 K. The experimental measurement of grain-swelling is reported for comparison sake.

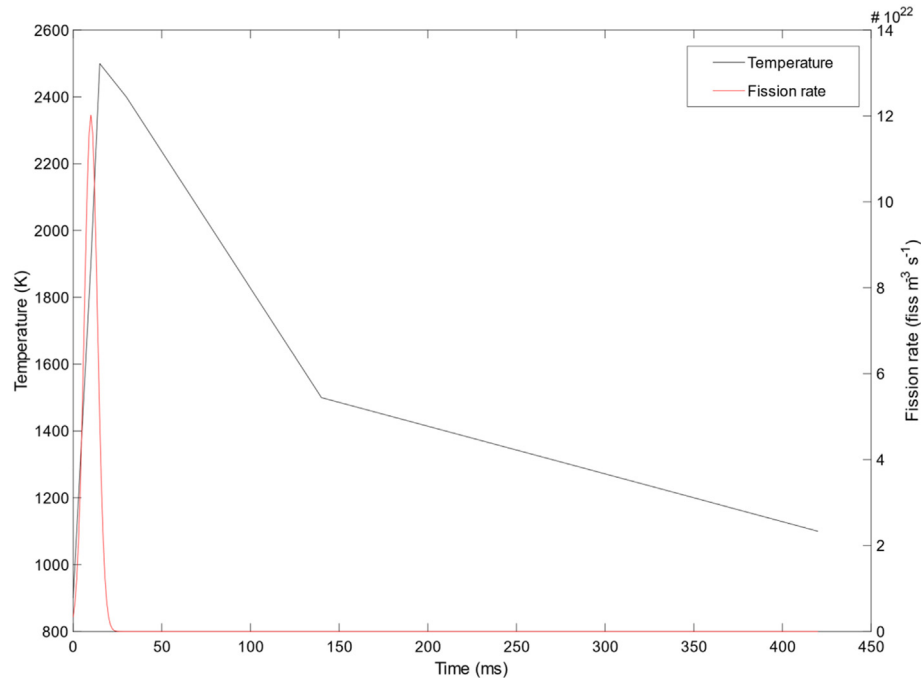


Fig. 10. Temperature and power histories of the CABRI REP Na-5 power pulse test [103].

Fig. 11 reports the fission gas release evolution as a function of temperature as calculated by SCIAINTIX. The release during the base irradiation is negligible compared to that obtained during the transient ( $\approx 2\%$ ). The release of fission gas during this transient is ascribed by the model to the micro-cracking of grain boundaries, and thus is predicted to occur during both the heat up and the cool down. The measured integral fission gas release for the CABRI REP-Na5 test transient was of 15.1% [103]. Besides this experimental result not being directly comparable with the 0D local result obtained with SCIAINTIX, it is in line with integral fuel performance calculations performed on the same RIA transient test applying a similar grain-boundary micro-cracking model [104].

As declared, the scope of this section is purely to demonstrate the suitability of SCIAINTIX in simulating transients in the scale of milliseconds: several model developments are required for a proper description of fission gas behaviour during RIA transient scenarios. Among the others, the treatment of non-equilibrium trapping and re-solution has been proved to play a role in this timescales [105].

## 5. Summary and future developments

As discussed in the previous Sections, in this work we presented the models currently available in the open source version of SCIAINTIX (available at [67]), together with a summary of the validation and selected showcases of results compared with experimental data (since the extensive validation of these models has been published independently [26,34,43,70]). Summarizing, the current version of SCIAINTIX:

- Is designed to be used effectively as a fission gas behaviour module included/coupled in/with fuel performance codes, and as stand-alone code as well.
- Includes a set of numerical solvers, each verified through the method of manufactured solutions, and has computational requirements in line with the needs of fuel performance codes.

- Includes a consistent set of models (independently published and validated) describing fission gas behaviour in  $\text{UO}_2$ , providing an overall physic-based description of the phenomena, with semi-empirical approaches used essentially for model parameters.

In view of these characteristics, SCIAINTIX is a candidate to effectively realize a multi-scale bridging in the description of fission gas behaviour in oxide fuel, allowing for the transfer of knowledge from the lower-length scale up to the engineering-scale of fuel performance codes<sup>18</sup>

- As conclusion, we summarize the ongoing model developments of SCIAINTIX: A description of helium behaviour, based on the current treatment of fission gas behaviour but including additional terms, such as the solubility [106–109]. This model is of relevance for the simulation of uranium-plutonium mixed oxide fuels and of storage conditions, where helium concentration becomes relevant.
- A description of actinide evolution with burnup, based on a reduced order model employing Bateman's equation with energy-averaged cross sections considered as functions of burnup and initial fuel composition [110–112]. This depletion capability implies the prediction of the helium production rate.
- A model describing intra-granular bubble coarsening, extending the model presented in this paper by adding an additional growth mechanism to bubbles close to dislocations [81]. This model will allow a more accurate description of intra-granular bubble swelling during transients.

<sup>18</sup> As an example, model parameters (like diffusivity of atoms and vacancies, re-solution and nucleation rate formulation) may be calculated by atomistic approaches, molecular dynamics, or other lower-length scale methods. Then, one may plug the derived expression in the current models, as an additional option beside available correlations, without affecting the evolution equations constituting the models.

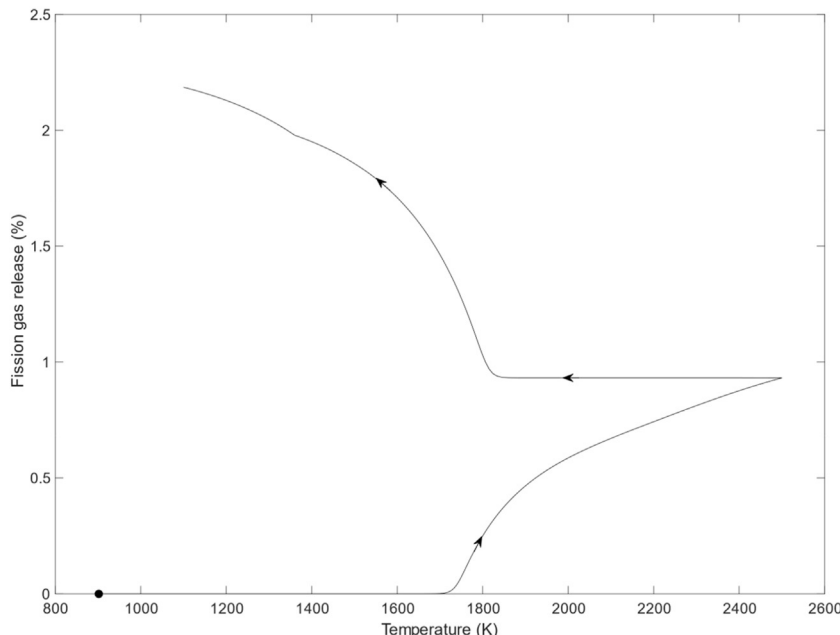


**Fig. 11.** Evolution of fission gas release as a function of temperature during the CABRI REP-Na5 transient test, as simulated by SCIAINTIX.

- A model describing the evolution of porosity in the high burnup structure [113,114], completing and extending the treatment of high burnup structure formation and depletion presented in this work, remarkably overcoming some semi-empirical approaches present in the current model.
- A reduced order model describing the diffusion of intra-granular gas in columnar grains [1], relevant for the simulation of MOX fuel in fast reactor conditions.

More long-term developments include the description of fission products formation and evolution, and the description of point defects evolution and interaction with fission gas. For all these model developments, the validation strategy based on comparison with separate effect experiments is going to be applied when possible.

As for the inclusion of SCIAINTIX within fuel performance codes as a fission gas behaviour module, the current status is that coupling has been demonstrated in TRANSURANUS [115] and will be subject of future publications, and is being pursued for GERMINAL code [116] in the frame of the INSPYRE Project [65].

#### Declaration of competing interest

The authors declare that they have no known competing financial interests or personal relationships that could have appeared to influence the work reported in this paper.

#### CRediT authorship contribution statement

**D. Pizzocri:** Conceptualization, Methodology, Software, Validation, Writing - original draft, Writing - review & editing, Visualization. **T. Barani:** Conceptualization, Methodology, Software, Validation, Writing - original draft, Writing - review & editing, Visualization. **L. Luzzi:** Conceptualization, Writing - original draft, Writing - review & editing, Project administration, Funding acquisition, Supervision.

#### Acknowledgments

The authors are grateful to the master and PhD students having contributed or currently working on the developments of SCIAINTIX at Politecnico di Milano: L. Cognini, A. Magni, S. Altieri, A.G. Carloni, A. Cechet, G. Rota, F. Verdolin.

This work has received funding from the Euratom research and training programme 2014–2018 through the INSPYRE project under grant agreement No 754329. This research contributes to the Joint Programme on Nuclear Materials (JPNM) of the European Energy Research Alliance (EERA), in the specific framework of the COMBATFUEL Project.

#### Appendix A. Supplementary data

Supplementary data to this article can be found online at <https://doi.org/10.1016/j.jnucmat.2020.152042>.

#### References

- [1] T. Motta, D.R. Olander, Light Water Reactor Materials, American Nuclear Society Scientific Publications, 2017.
- [2] P. Van Uffelen, R.J.M. Konings, C. Vitanza, J. Tulenko, Analysis of reactor fuel rod behavior, in: D.G. Cacuci (Ed.), Handb. Nucl. Eng., Springer Science + Business Media, LLC, New York, NY, USA, 2010, pp. 1519–1627.
- [3] P. Van Uffelen, J. Hales, W. Li, G. Rossiter, R. Williamson, A review of fuel performance modelling, J. Nucl. Mater. 516 (2019) 373–412, <https://doi.org/10.1016/j.jnucmat.2018.12.037>.
- [4] K. Lassmann, TRANSURANUS: a fuel rod analysis code ready for use, J. Nucl. Mater. 188 (1992) 295–302, [https://doi.org/10.1016/0022-3115\(92\)90487-6](https://doi.org/10.1016/0022-3115(92)90487-6).
- [5] H.S. Aybar, P. Ortego, A review of nuclear fuel performance codes, Prog. Nucl. Energy 46 (2005) 127–141, <https://doi.org/10.1016/j.pnucene.2005.01.004>.
- [6] M.E. Cunningham, C.E. Beyer, P.G. Medvedev, G.A. Berna, FRAPTRAN: a computer code for the transient analysis of oxide fuel rods, Nureg/cr 6739 (2001) 1.
- [7] J.Y.R. Rashid, S.K. Yagnik, R.O. Montgomery, Light water reactor fuel performance modeling and multi-dimensional simulation, JOM (J. Miner. Metals Mater. Soc.) 63 (2011) 81, <https://doi.org/10.1007/s11837-011-0144-9>.
- [8] K. Lassmann, The structure of fuel element codes, Nucl. Eng. Des. 57 (1980) 17–39, [https://doi.org/10.1016/0029-5493\(80\)90221-6](https://doi.org/10.1016/0029-5493(80)90221-6).
- [9] J. Sercombe, E. Féderici, M. Le Saux, B. Michel, C. Poussard, 1D and 3D

- modeling of PCMI during a RIA with ALCYONE V1. 1, in: Int. Top. Meet. Light Water React. Fuel Performance, Orlando, Florida, 2010.
- [10] R.L. Williamson, J.D. Hales, S.R. Novascone, M.R. Tonks, D.R. Gaston, C.J. Perrmann, D. Andrs, R.C. Martineau, Multidimensional multiphysics simulation of nuclear fuel behavior, *J. Nucl. Mater.* 423 (2012) 149–163, <https://doi.org/10.1016/j.jnucmat.2012.01.012>.
- [11] M. Tonks, D. Andersson, R. Devathanan, R. Dubourg, A. El-Azab, M. Freyss, F. Iglesias, K. Kulacsy, G. Pastore, S.R. Phillipot, M. Welland, Unit mechanisms of fission gas release: current understanding and future needs, *J. Nucl. Mater.* 504 (2018) 300–317, <https://doi.org/10.1016/j.jnucmat.2018.03.016>.
- [12] J. Rest, M.W.D. Cooper, J. Spino, J.A. Turnbull, P. Van Uffelen, C.T. Walker, Fission gas release from  $\text{UO}_2$  nuclear fuel: a review, *J. Nucl. Mater.* 513 (2019) 310–345, <https://doi.org/10.1016/j.jnucmat.2018.08.019>.
- [13] K. Lassmann, H. Benk, Numerical algorithms for intragranular fission gas release, *J. Nucl. Mater.* 280 (2000) 127–135, [https://doi.org/10.1016/S0022-3115\(00\)00044-1](https://doi.org/10.1016/S0022-3115(00)00044-1).
- [14] A. Denis, R. Piotrkowski, Simulation of isothermal fission gas release, *J. Nucl. Mater.* 229 (1996) 149–154, [https://doi.org/10.1016/0022-3115\(95\)00203-0](https://doi.org/10.1016/0022-3115(95)00203-0).
- [15] G.A. Berna, C.E. Beyer, K.L. Davis, D.D. Lanning, P. Northwest, FRAPCON-3 : A Computer Code for the Calculation of Steady-State , Thermal- Mechanical Behavior of Oxide Fuel Rods for, 1997, p. 2.
- [16] J.P. Foster, S. Sidener, Westinghouse Improved Performance Analysis and Design Model (PAD 4.0), 2000.
- [17] L.C. Bernard, J.L. Jacoud, P. Vesco, An efficient model for the analysis of fission gas release, *J. Nucl. Mater.* 302 (2002) 125–134, [https://doi.org/10.1016/S0022-3115\(02\)00793-6](https://doi.org/10.1016/S0022-3115(02)00793-6).
- [18] Á. Griger, J. Gadó, Models of the FUROM-1.3 Code, 2007.
- [19] A.R. Massih, K. Forsberg, Calculation of grain boundary gaseous swelling in  $\text{UO}_2$ , *J. Nucl. Mater.* 377 (2008) 406–408, <https://doi.org/10.1016/j.jnucmat.2008.03.011>.
- [20] J.A. Turnbull, C.E. Beyer, Background and Derivation of ANS-5 . 4 Standard Fission Product Release Model, United States Nucl. Regul. Commision., 2010, p. 11.
- [21] K. Mikityuk, A. Shestopalov, FRED fuel behaviour code: main models and analysis of Halden IFA-503.2 tests, *Nucl. Eng. Des.* 241 (2011) 2455–2461, <https://doi.org/10.1016/j.nucengdes.2011.04.033>.
- [22] R.J. White, M.O. Tucker, A new fission-gas release model, *J. Nucl. Mater.* 118 (1983) 1–38, [https://doi.org/10.1016/0022-3115\(83\)90176-9](https://doi.org/10.1016/0022-3115(83)90176-9).
- [23] J. Rest, An improved model for fission product behavior in nuclear fuel under normal and accident conditions, *J. Nucl. Mater.* 120 (1984) 195–212, [https://doi.org/10.1016/0022-3115\(84\)90057-6](https://doi.org/10.1016/0022-3115(84)90057-6).
- [24] M.S. Veshchunov, V.I. Tarasov, Modelling of irradiated  $\text{UO}_2$  fuel behaviour under transient conditions, *J. Nucl. Mater.* 437 (2013) 250–260, <https://doi.org/10.1016/j.jnucmat.2013.02.011>.
- [25] G. Jomard, C. Struzik, A. Boulore, P. Mailhé, V. Auret, R. Largentton, CARACAS : an Industrial Model for the Description of Fission Gas Behavior in LWR- $\text{UO}_2$  Fuel, 2014, pp. 14–17.
- [26] D. Pizzocri, G. Pastore, T. Barani, A. Magni, L. Luzzi, P. Van Uffelen, S.A. Pitts, A. Alfonsi, J.D. Hales, A model describing intra-granular fission gas behaviour in oxide fuel for advanced engineering tools, *J. Nucl. Mater.* 502 (2018), <https://doi.org/10.1016/j.jnucmat.2018.02.024>.
- [27] J. Rest, A. Zawadzki, reportFASTGRASS : A Mechanistic Model for the Prediction of Xe , I , Cs , Te , Ba, and Sr Release from Nuclear Fuel under Normal and Severe-Accident Conditions, (n.d.) Report NUREG/CR-5840.
- [28] P. Van Uffelen, Contribution to the Modelling of Fission Gas Release in Light Water Reactor Fuel, Université de Liège, 2002.
- [29] P. Löösönen, Modelling intragranular fission gas release in irradiation of sintered LWR  $\text{UO}_2$  fuel, *J. Nucl. Mater.* 304 (2002) 29–49, [https://doi.org/10.1016/S0022-3115\(02\)00856-5](https://doi.org/10.1016/S0022-3115(02)00856-5).
- [30] R.J. White, The development of grain-face porosity in irradiated oxide fuel, *J. Nucl. Mater.* 325 (2004) 61–77, <https://doi.org/10.1016/j.jnucmat.2003.10.008>.
- [31] M.S. Veshchunov, V.D. Ozrin, V.E. Shestak, V.I. Tarasov, R. Dubourg, G. Nicaise, Development of the mechanistic code MFPR for modelling fission-product release from irradiated  $\text{UO}_2$  fuel, *Nucl. Eng. Des.* 236 (2006) 179–200, <https://doi.org/10.1016/j.nucengdes.2005.08.006>.
- [32] G. Khvostov, K. Mikityuk, M.A. Zimmermann, A model for fission gas release and gaseous swelling of the uranium dioxide fuel coupled with the FALCON code, *Nucl. Eng. Des.* 241 (2011) 2983–3007, <https://doi.org/10.1016/j.nucengdes.2011.06.020>.
- [33] L. Noiroit, MARGARET: a comprehensive code for the description of fission gas behavior, *Nucl. Eng. Des.* 241 (2011) 2099–2118, <https://doi.org/10.1016/j.nucengdes.2011.03.044>.
- [34] G. Pastore, L. Luzzi, V. Di Marcello, P. Van Uffelen, Physics-based modelling of fission gas swelling and release in  $\text{UO}_2$  applied to integral fuel rod analysis, *Nucl. Eng. Des.* 256 (2013) 75–86, <https://doi.org/10.1016/j.nucengdes.2012.12.002>.
- [35] B.T. Kelly, The application of chemical rate theory to fast neutron irradiation damage in graphite, *Carbon* 14 (1976) 239–245, [https://doi.org/10.1016/0008-6223\(76\)90115-9](https://doi.org/10.1016/0008-6223(76)90115-9).
- [36] A.D. Brailsford, R. Bulloough, The rate theory of swelling due to void growth in irradiated metals, *J. Nucl. Mater.* 44 (1972) 121–135, [https://doi.org/10.1016/0022-3115\(72\)90091-8](https://doi.org/10.1016/0022-3115(72)90091-8).
- [37] M.R. Tonks, D. Andersson, S.R. Phillipot, Y. Zhang, R. Williamson, C.R. Stanek, B.P. Uberuaga, S.L. Hayes, Mechanistic materials modeling for nuclear fuel performance, *Ann. Nucl. Energy* 105 (2017) 11–24, <https://doi.org/10.1016/J.JANUCENE.2017.03.005>.
- [38] D. Yun, J. Rest, G.L. Hofman, A.M. Yacout, An initial assessment of a mechanistic model, GRASS-SST, in U-Pu-Zr metallic alloy fuel fission-gas behavior simulations, *J. Nucl. Mater.* 435 (2013) 153–163, <https://doi.org/10.1016/j.jnucmat.2012.12.024>.
- [39] J. Rest, A generalized model for radiation-induced amorphization and crystallization of  $\text{U}_3\text{Si}$  and  $\text{U}_3\text{Si}_2$  and recrystallization of  $\text{UO}_2$ , *J. Nucl. Mater.* 248 (1997) 205–214.
- [40] J. Rest, A model for the influence of microstructure, precipitate pinning and fission gas behavior on irradiation-induced recrystallization of nuclear fuels, *J. Nucl. Mater.* 326 (2004) 175–184, <https://doi.org/10.1016/j.jnucmat.2004.01.009>.
- [41] J.H. Evans, Bubble diffusion to grain boundaries in  $\text{UO}_2$  and metals during annealing: a new approach, *J. Nucl. Mater.* 210 (1994) 21–29.
- [42] M.S. Veshchunov, V.E. Shestak, Modelling of fission gas release from irradiated  $\text{UO}_2$  fuel under high-temperature annealing conditions, *J. Nucl. Mater.* 430 (2012) 82–89, <https://doi.org/10.1016/j.jnucmat.2012.06.048>.
- [43] T. Barani, E. Bruschi, D. Pizzocri, G. Pastore, P. Van Uffelen, R.L. Williamson, L. Luzzi, Analysis of transient fission gas behaviour in oxide fuel using BISON and TRANSURANUS, *J. Nucl. Mater.* 486 (2017), <https://doi.org/10.1016/j.jnucmat.2016.10.051>.
- [44] M. Stan, Discovery and design of nuclear fuels, *Mater. Today* 12 (2009) 20–28, [https://doi.org/10.1016/S1369-7021\(09\)70295-0](https://doi.org/10.1016/S1369-7021(09)70295-0).
- [45] E.A. Kotomin, Y.A. Mastrikov, S.N. Rashkeev, P. Van Uffelen, Implementing first principles calculations of defect migration in a fuel performance code for UN simulations, *J. Nucl. Mater.* 393 (2009) 292–299, <https://doi.org/10.1016/j.jnucmat.2009.06.016>.
- [46] D.A. Andersson, P. Garcia, X.Y. Liu, G. Pastore, M. Tonks, P. Millett, B. Dorado, D.R. Gaston, D. Andrs, R.L. Williamson, R.C. Martineau, B.P. Uberuaga, C.R. Stanek, Atomistic modeling of intrinsic and radiation-enhanced fission gas (Xe) diffusion in  $\text{UO}_2$   $\pm x$ : implications for nuclear fuel performance modeling, *J. Nucl. Mater.* 451 (2014) 225–242, <https://doi.org/10.1016/j.jnucmat.2014.03.041>.
- [47] M. Bertolus, M. Freyss, B. Dorado, G. Martin, K. Hoang, S. Maillard, R. Skorek, P. Garcia, C. Valot, A. Chartier, L. Van Brutzel, P. Fossati, R.W. Grimes, D.C. Parfitt, C.L. Bishop, S.T. Murphy, M.J.D. Rushton, D. Staicu, E. Yakub, S. Nichenko, M. Krack, F. Devynck, R. Ngayam-Happy, K. Govers, C.S. Deo, R.K. Behera, Linking atomic and mesoscopic scales for the modelling of the transport properties of uranium dioxide under irradiation, *J. Nucl. Mater.* 462 (2015) 475–495, <https://doi.org/10.1016/j.jnucmat.2015.02.026>.
- [48] M.R. Tonks, X.Y. Liu, D. Andersson, D. Perez, A. Chernatynskiy, G. Pastore, C.R. Stanek, R. Williamson, Development of a multiscale thermal conductivity model for fission gas in  $\text{UO}_2$ , *J. Nucl. Mater.* 469 (2016) 89–98, <https://doi.org/10.1016/j.jnucmat.2015.11.042>.
- [49] X.M. Bai, M.R. Tonks, Y. Zhang, J.D. Hales, Multiscale modeling of thermal conductivity of high burnup structures in  $\text{UO}_2$  fuels, *J. Nucl. Mater.* 470 (2016) 208–215, <https://doi.org/10.1016/j.jnucmat.2015.12.028>.
- [50] Y. Miao, K.A. Gamble, D. Andersson, B. Ye, Z.G. Mei, G. Hofman, A.M. Yacout, Gaseous swelling of  $\text{U}_3\text{Si}_2$  during steady-state LWR operation: a rate theory investigation, *Nucl. Eng. Des.* 322 (2017) 336–344, <https://doi.org/10.1016/j.nucengdes.2017.07.008>.
- [51] T. Barani, G. Pastore, D. Pizzocri, D.A. Andersson, C. Matthews, A. Alfonsi, K.A. Gamble, P. Van Uffelen, L. Luzzi, J.D. Hales, Multiscale modeling of fission gas behavior in  $\text{U}_3\text{Si}_2$  under LWR conditions, *J. Nucl. Mater.* 522 (2019) 97–110, <https://doi.org/10.1016/j.jnucmat.2019.04.037>.
- [52] Y.-H. Koo, B.-H. Lee, D.-S. Sohn, Cosmos: a computer code to analyze LWR  $\text{UO}_2$  and MOX fuel up to high burnup, *Ann. Nucl. Energy* 26 (1999) 47–67, [https://doi.org/10.1016/S0306-4549\(98\)00033-4](https://doi.org/10.1016/S0306-4549(98)00033-4).
- [53] C.B. Lee, Y.S. Yang, D.H. Kim, S.K. Kim, J.G. Bang, A new mechanistic and engineering fission gas release model for a uranium dioxide fuel, *J. Nucl. Sci. Technol.* 45 (2008) 60–71, <https://doi.org/10.1080/18811248.2008.9711415>.
- [54] G. Rossiter, Development of the ENIGMA fuel performance code for whole core analysis and dry storage assessments, *Nucl. Eng. Technol.* 43 (2011) 489–498, <https://doi.org/10.5516/NET.2011.43.6.489>.
- [55] J.D. Hales, R.L. Williamson, S.R. Novascone, G. Pastore, B.W. Spencer, D.S. Stafford, K.A. Gamble, D.M. Perez, R.J. Gardner, B.W. Liu, BISON Theory Manual: the Quations behind Nuclear Fuel Analysis, Idaho Falls, ID, USA, 2014.
- [56] K. Lassmann, A. Schubert, P. Van Uffelen, C. Gyori, J. Van De Laar, TRANSURANUS Handbook, Karlsruhe, Germany, 2014.
- [57] G. Pastore, L.P. Swiler, J.D. Hales, S.R. Novascone, D.M. Perez, B.W. Spencer, L. Luzzi, P. Van Uffelen, R.L. Williamson, Uncertainty and sensitivity analysis of fission gas behavior in engineering-scale fuel modeling, *J. Nucl. Mater.* 456 (2015) 398–408, <https://doi.org/10.1016/j.jnucmat.2014.09.077>.
- [58] P. van Uffelen, G. Pastore, V. di Marcello, L. Luzzi, Multiscale modelling for the fission gas behaviour in the TRANSURANUS code, *Nucl. Eng. Technol.* 43 (2011) 477–488, <https://doi.org/10.5516/NET.2011.43.6.477>.
- [59] B. Baurens, J. Sercombe, C. Riglet-Martial, L. Desgranges, L. Trotignon, P. Maugis, 3D thermo-chemical-mechanical simulation of power ramps with ALCYONE fuel code, *J. Nucl. Mater.* 452 (2014) 578–594, <https://doi.org/10.1016/j.jnucmat.2014.06.021>.
- [60] G. Khvostov, Models for numerical simulation of burst FGR in fuel rods under the conditions of RIA, *Nucl. Eng. Des.* 328 (2018) 36–57, <https://doi.org/10.1016/j.nucengdes.2018.03.030>.

- 10.1016/J.NUCENGDES.2017.12.028.
- [61] Y. Rashid, R. Dunham, R. Montgomery, Fuel Analysis and Licensing Code: FALCON MOD01 Volume 1: Theoretical and Numerical Bases, vol. 1, 2004, p. 246.
- [62] M.S. Veshchunov, A.V. Boldyrev, V.D. Ozrin, V.E. Shestak, V.I. Tarasov, A new mechanistic code SFPR for modeling of single fuel rod performance under various regimes of LWR operation, *Nucl. Eng. Des.* 241 (2011) 2822–2830.
- [63] M.S. Veshchunov, A.V. Boldyrev, A.V. Kuznetsov, V.D. Ozrin, M.S. Seryi, V.E. Shestak, V.I. Tarasov, G.E. Norman, A.Y. Kuksin, V.V. Pisarev, D.E. Smirnova, S.V. Starikov, V.V. Stegailov, A.V. Yanilkin, Development of the advanced mechanistic fuel performance and safety code using the multi-scale approach, *Nucl. Eng. Des.* 295 (2015) 116–126, <https://doi.org/10.1016/j.nucengdes.2015.09.035>.
- [64] OECD-NEA NSC, State-of-the-Art Report on Multi-Scale Modelling of Nuclear Fuels, Organ. Econ. Co-Operation Dev., 2015, p. 380.
- [65] M. Bertolus, INSPYRE: Investigations Supporting MOX Fuel Licensing in ESNII Prototype Reactors, 2017. <http://www.eera-jpnm.eu/inspyre/>.
- [66] B.D. Wirth, Fission Gas SciDAC 4: Simulation of Fission Gas in Uranium Oxide Nuclear Fuel, 2018. <https://collab.cels.anl.gov/display/FissionGasSciDAC2>.
- [67] D. Pizzocri, T. Barani, L. Luzzi, SCIANTIX code, Online Repos. (n.d.). <https://gitlab.com/polimirng/sciantix> (accessed October 4, 2019).
- [68] K. Salari, P. Knupp, Code Verification by the Method of Manufactured Solutions, 2000.
- [69] W.L. Oberkampf, T.G. Trucano, Verification and validation in computational fluid dynamics.pdf, *Prog. Aero. Sci.* 38 (2002) 209–272, [https://doi.org/10.1016/S0376-0421\(02\)00005-2](https://doi.org/10.1016/S0376-0421(02)00005-2).
- [70] D. Pizzocri, F. Cappia, L. Luzzi, G. Pastore, V.V. Rondinella, P. Van Uffelen, A semi-empirical model for the formation and the depletion of the high burnup structure in  $\text{UO}_2$  fuel, *J. Nucl. Mater.* 487 (2017) 23–29.
- [71] T. Wiss, V.V. Rondinella, R.J.M. Konings, D. Staicu, D. Papaioannou, S. Bremier, P. Pöml, O. Benes, J.-Y. Colle, P. Van Uffelen, A. Schubert, F. Cappia, M. Marchetti, D. Pizzocri, F. Jatuff, W. Goll, T. Sonoda, A. Sasahara, S. Kitajima, M. Kinoshita, Properties of the high burnup structure in nuclear light water reactor fuel, *Radiochim. Acta* 105 (2017), <https://doi.org/10.1515/ract-2017-2831>.
- [72] D.R. Olander, D. Wongswaeng, Re-solution of fission gas – a review: Part I. Intragranular bubbles, *J. Nucl. Mater.* 354 (2006) 94–109, <https://doi.org/10.1016/j.jnucmat.2006.03.010>.
- [73] A.M. Booth, A Method of Calculating Fission Gas Diffusion from  $\text{UO}_2$  Fuel and its Application to the X-2-F Loop Test, 1957.
- [74] M.V. Speight, A calculation on the migration of fission gas in material exhibiting precipitation and Re-solution of gas atoms under irradiation, *Nucl. Sci. Eng.* 37 (1969) 180–185, <https://doi.org/10.13182/nse69-a20676>.
- [75] J. Turnbull, R. White, C. Wise, The diffusion coefficient for fission gas atoms in uranium dioxide, in: Proc. a Tech. Comm. Meet. Organ. by Int. At. Energy Agency Held Preston, 18–22 Sept. 1988, 1989.
- [76] H. Matzke, Gas release mechanisms in  $\text{UO}_2$  – a critical review, *Radiat. Eff.* 53 (1980) 219–242.
- [77] J.A. Turnbull, The distribution of intragranular fission gas bubbles in  $\text{UO}_2$  during irradiation, *J. Nucl. Mater.* 38 (1971) 203–212.
- [78] F.S. Ham, Theory of diffusion-limited precipitation, *J. Phys. Chem. Solid.* 6 (1958) 335–351.
- [79] C. Baker, The fission gas bubble distribution in uranium dioxide from high temperature irradiated SGHWR fuel pins, *J. Nucl. Mater.* 66 (1977) 283–291, [https://doi.org/10.1016/0022-3115\(77\)90195-7](https://doi.org/10.1016/0022-3115(77)90195-7).
- [80] G. Pastore, D. Pizzocri, J.D. Hales, S.R. Novascone, R.L. Williamson, B.W. Spencer, Modeling of transient fission gas behavior in oxide fuel and application to the BISON code, *Proc. Enlarg. Halden Program. Gr. Meet. Roros, Norw.* (2014) 12–16.
- [81] R.J. White, R.C. Corcoran, P.J. Barnes, A Summary of Swelling Data Obtained from the AGR/Halden Ramp Test Programme, 2006, pp. 1–192.
- [82] M.V. Speight, W. Beere, Vacancy potential and void growth on grain boundaries, *Acta Met. Soc.* 9 (1975) 190–191.
- [83] M.J.F. Notley, J.R. MacEwan, Stepwise release of fission gas from  $\text{UO}_2$  fuel, *Nucl. Appl.* 2 (1966) 477–480, <https://doi.org/10.13182/nt66-a27540>.
- [84] R.M. Carroll, J.G. Morgan, R.B. Perez, O. Sisman, Fission density, burnup, and temperature effects on fission-gas release from  $\text{UO}_2$ , *Nucl. Sci. Eng.* 38 (1969) 143–155, <https://doi.org/10.13182/nse69-a19519>.
- [85] U. Katsumi, K. Shinji, Fission gas release during post irradiation annealing of bwr fuels, *J. Nucl. Sci. Technol.* 27 (1990) 1002–1016, <https://doi.org/10.1080/18811248.1990.9731285>.
- [86] G. Ducros, Y. Pontillon, P.P. Malgouyres, Synthesis of the VERCORS experimental programme: separate-effect experiments on fission Product release, in support of the PHEBUS-FP programme, *Ann. Nucl. Energy* 61 (2013) 75–87, <https://doi.org/10.1016/j.anucene.2013.02.033>.
- [87] W. Hering, The kww fission gas release model for lwr fuel rods, *J. Nucl. Mater.* 114 (1983) 41–49, [https://doi.org/10.1016/0022-3115\(83\)90071-5](https://doi.org/10.1016/0022-3115(83)90071-5).
- [88] G.L. Reynolds, B. Burton, Grain-boundary diffusion in uranium dioxide: the correlation between sintering and creep and a reinterpretation of creep mechanism, *J. Nucl. Mater.* 82 (1979) 22–25.
- [89] R. Hargreaves, D.A. Collins, A quantitative model for fission gas release and swelling in irradiated uranium dioxide, *J. Br. Nucl. Energy Soc.* 15 (1976) 311–318.
- [90] M.J.F. Notley, I.J. Hastings, A microstructure-dependent model for fission product gas release and swelling in  $\text{UO}_2$  fuel, *Nucl. Eng. Des.* 56 (1980) 163–175, [https://doi.org/10.1016/0029-5493\(80\)90180-6](https://doi.org/10.1016/0029-5493(80)90180-6).
- [91] T. Kogai, Modelling of fission gas release and gaseous swelling of light water reactor fuels, *J. Nucl. Mater.* 244 (1997) 131–140, [https://doi.org/10.1016/S0022-3115\(96\)00731-3](https://doi.org/10.1016/S0022-3115(96)00731-3).
- [92] P. Botazzoli, Helium Production and Behaviour in LWR Oxide Nuclear Fuels, Ph.D Thesis, Politec. Di Milano, Italy, 2011.
- [93] P. Van Uffelen, P. Botazzoli, L. Luzzi, S. Bremier, A. Schubert, P. Raison, R. Eloirdi, M.A. Barker, An experimental study of grain growth in mixed oxide samples with various microstructures and plutonium concentrations, *J. Nucl. Mater.* 434 (2013) 287–290, <https://doi.org/10.1016/j.jnucmat.2012.11.053>.
- [94] M. Hillert, On the theory of normal and abnormal grain growth, *Acta Metall.* 13 (1965) 227–238, [https://doi.org/10.1016/0001-6160\(65\)90200-2](https://doi.org/10.1016/0001-6160(65)90200-2).
- [95] J.B. Ainscough, B.W. Oldfield, J.O. Ware, Isothermal grain growth kinetics in sintered  $\text{UO}_2$  pellets, *J. Nucl. Mater.* 49 (1973) 117–128, [https://doi.org/10.1016/0022-3115\(73\)90001-9](https://doi.org/10.1016/0022-3115(73)90001-9).
- [96] J.E. Bainbridge, C.B.A. Forty, D.G. Martin, The grain growth of mixed oxide fuel during irradiation, *J. Nucl. Mater.* 171 (1990) 230–236, [https://doi.org/10.1016/0022-3115\(90\)90370-3](https://doi.org/10.1016/0022-3115(90)90370-3).
- [97] M.S. Veshchunov, A new model of grain growth kinetics in  $\text{UO}_2$  fuel pellets. Part 2: normal grain growth kinetics controlled by pore migration, *J. Nucl. Mater.* 346 (2005) 220–225, <https://doi.org/10.1016/j.jnucmat.2005.06.010>.
- [98] I.L.F. Ray, H. Matzke, H.A. Thiele, M. Kinoshita, An electron microscopy study of the RIM structure of a  $\text{UO}_2$  fuel with a high burnup of 7.9% FIMA, *J. Nucl. Mater.* 245 (1997) 115–123, [https://doi.org/10.1016/S0022-3115\(97\)00015-9](https://doi.org/10.1016/S0022-3115(97)00015-9).
- [99] J. Noiroit, L. Desgranges, J. Lamontagne, Detailed characterisations of high burn-up structures in oxide fuels, *J. Nucl. Mater.* 372 (2008) 318–339, <https://doi.org/10.1016/j.jnucmat.2007.04.037>.
- [100] V.V. Rondinella, T. Wiss, The high burn-up structure in nuclear fuel, *Mater. Today* 13 (2010) 24–32, [https://doi.org/10.1016/S1369-7021\(10\)70221-2](https://doi.org/10.1016/S1369-7021(10)70221-2).
- [101] L. Holt, A. Schubert, P. Van Uffelen, C.T. Walker, E. Fridman, T. Sonoda, Sensitivity study on Xe depletion in the high burn-up structure of  $\text{UO}_2$ , *J. Nucl. Mater.* 452 (2014) 166–172, <https://doi.org/10.1016/j.jnucmat.2014.05.009>.
- [102] G. Pastore, T. Barani, D. Pizzocri, A. Magni, L. Luzzi, Modeling fission gas release and bubble evolution in  $\text{UO}_2$  for engineering fuel rod analysis, in: *Top Fuel*, 2018, pp. 1–8. Prague, 2019.
- [103] NEA/CSNI/R, Nuclear Fuel Behaviour under Reactivity-Initiated Accident, 1, (RIA) Conditions, 2010, 2010.
- [104] G. Pastore, C.P. Folsom, R.L. Williamson, J.D. Hales, L. Luzzi, D. Pizzocri, T. Barani, Modeling fission gas behavior with the BISON fuel performance code, in: *EHPG Meet. Lillehammer, Norway*, 24–29 Sep 2017, 2017.
- [105] G. Pastore, D. Pizzocri, C. Rabiti, T. Barani, P. Van Uffelen, L. Luzzi, An effective numerical algorithm for intra-granular fission gas release during non-equilibrium trapping and resolution, *J. Nucl. Mater.* 509 (2018) 687–699, <https://doi.org/10.1016/j.jnucmat.2018.07.030>.
- [106] D.R. Olander, Theory of helium dissolution in uranium dioxide. II. Helium solubility, *J. Chem. Phys.* 43 (1965) 785–788, <https://doi.org/10.1063/1.1696844>.
- [107] E. Maugeri, T. Wiss, J.P. Hiernaut, K. Desai, C. Thiriet, V.V. Rondinella, J.Y. Colle, R.J.M. Konings, Helium solubility and behaviour in uranium dioxide, *J. Nucl. Mater.* 385 (2009) 461–466, <https://doi.org/10.1016/j.jnucmat.2008.12.033>.
- [108] L. Noiroit, A method to calculate equilibrium concentrations of gas and defects in the vicinity of an over-pressured bubble in  $\text{UO}_2$ , *J. Nucl. Mater.* 447 (2014) 166–178, <https://doi.org/10.1016/j.jnucmat.2014.01.011>.
- [109] L. Cognini, D. Pizzocri, T. Barani, P. Van Uffelen, A. Schubert, T. Wiss, L. Luzzi, Helium solubility in oxide nuclear fuel: derivation of new correlations for Henry's constant, *Nucl. Eng. Des.* 340 (2018) 240–244, <https://doi.org/10.1016/j.nucengdes.2018.09.024>.
- [110] K. Lassmann, C. O'Carroll, J. van de Laar, C.T. Walker, The radial distribution of plutonium in high burnup  $\text{UO}_2$  fuels, *J. Nucl. Mater.* 208 (1994) 223–231, [https://doi.org/10.1016/0022-3115\(94\)90331-X](https://doi.org/10.1016/0022-3115(94)90331-X).
- [111] K. Lassmann, C.T. Walker, J. van de Laar, Extension of the TRANSURANUS burnup model to heavy water reactor conditions, *J. Nucl. Mater.* 255 (1998) 222–233, [https://doi.org/10.1016/S0022-3115\(98\)00019-1](https://doi.org/10.1016/S0022-3115(98)00019-1).
- [112] A. Schubert, P. Van Uffelen, J. van de Laar, C.T. Walker, W. Haack, Extension of the TRANSURANUS burn-up model, *J. Nucl. Mater.* 376 (2008) 1–10, <https://doi.org/10.1016/j.jnucmat.2008.01.006>.
- [113] J. Spino, A.D. Stalios, H. Santa Cruz, D. Baron, Stereological evolution of the rim structure in PWR-fuels at prolonged irradiation: dependencies with burn-up and temperature, *J. Nucl. Mater.* 354 (2006) 66–84, <https://doi.org/10.1016/j.jnucmat.2006.02.095>.
- [114] F. Cappia, D. Pizzocri, A. Schubert, P. Van Uffelen, G. Paperini, D. Pellottiero, R. Macián-Juan, V.V. Rondinella, Critical assessment of the pore size distribution in the rim region of high burnup  $\text{UO}_2$  fuels, *J. Nucl. Mater.* 480 (2016), <https://doi.org/10.1016/j.jnucmat.2016.08.010>.
- [115] D. Pizzocri, T. Barani, L. Luzzi, Coupling of TRANSURANUS with the SCIANTIX fission gas behaviour module, in: *Int. Work. "Towar. Nucl. Fuel Model. Var. React. Types across Eur.*, 2019.
- [116] M. Lainet, B. Michel, J.C. Dumas, M. Pelletier, I. Ramière, GERMINAL, a fuel performance code of the PLEIADES platform to simulate the in-pile behaviour of mixed oxide fuel pins for sodium-cooled fast reactors, *J. Nucl. Mater.* 516 (2019) 30–53, <https://doi.org/10.1016/j.jnucmat.2018.12.030>.

- [117] K. Forsberg, A. Massih, Diffusion theory of fission gas migration in irradiated nuclear fuel  $\text{UO}_2$ , *J. Nucl. Mater.* 135 (1985) 140–148.
- [118] D. Pizzocri, C. Rabiti, L. Luzzi, T. Barani, P. Van Uffelen, G. Pastore, PolyPole-1: an accurate numerical algorithm for intra-granular fission gas release, *J. Nucl. Mater.* 478 (2016), <https://doi.org/10.1016/j.jnucmat.2016.06.028>.
- [119] MOOSE platform (Multiphysics Object Oriented Simulation Environment), (n.d.), <https://mooseframework.org/>.
- [120] C. Baker, The migration of intragranular fission gas bubbles in irradiated uranium dioxide, *J. Nucl. Mater.* 71 (1977) 117–123, [https://doi.org/10.1016/0022-3115\(77\)90195-7](https://doi.org/10.1016/0022-3115(77)90195-7).
- [121] L. Verma, L. Noirot, P. Maugis, A new spatially resolved model for defects and fission gas bubbles interaction at the mesoscale, *Nucl. Instrum. Methods Phys. Res. B* 458 (2019) 151–158, <https://doi.org/10.1016/j.nimb.2018.10.028>.
- [122] L. Verma, L. Noirot, P. Maugis, Modelling intra-granular bubble movement and fission gas release during post-irradiation annealing of  $\text{UO}_2$  using meso-scale and spatialized approach, *J. Nucl. Mater.* 528 (2020).
- [123] L.E. Thomas, Condensed-phase xenon and krypton in  $\text{UO}_2$  spent fuel, in: S.E. Donnelly, J.H. Evans (Eds.), *Fundam. Asp. Inert Gases Solids*, Springer US, 1991, pp. 431–441.
- [124] K. Nogita, K. Ume, High resolution TEM observation and density estimation of Xe bubbles in high burnup  $\text{UO}_2$  fuels, *Nucl. Instrum. Methods Phys. Res. Sect. B Beam Interact. Mater. Atoms* 141 (1998) 481–486, [https://doi.org/10.1016/S0168-583X\(98\)00040-8](https://doi.org/10.1016/S0168-583X(98)00040-8).
- [125] J. Spino, J. Rest, W. Goll, C.T. Walker, Matrix swelling rate and cavity volume balance of  $\text{UO}_2$  fuels at high burn-up, *J. Nucl. Mater.* 346 (2005) 131–144, <https://doi.org/10.1016/j.jnucmat.2005.06.015>.
- [126] C. Ronchi, Extrapolated equation of state for rare gases at high temperatures and densities, *J. Nucl. Mater.* 96 (1981) 314–328, [https://doi.org/10.1016/0022-3115\(81\)90575-4](https://doi.org/10.1016/0022-3115(81)90575-4).
- [127] J. Rest, The effect of irradiation-induced gas-atom re-solution on grain-boundary bubble growth, *J. Nucl. Mater.* 321 (2003) 305–312, [https://doi.org/10.1016/S0022-3115\(03\)00303-9](https://doi.org/10.1016/S0022-3115(03)00303-9).
- [128] M.R. Tonks, Y. Zhang, X. Bai, P.C. Millett, Demonstrating the temperature gradient impact on grain growth in  $\text{UO}_2$  using the phase field method, *Mater. Res. Lett.* 2 (2014) 23–28, <https://doi.org/10.1080/21663831.2013.849300>.
- [129] X.-M. Bai, Y. Zhang, M.R. Tonks, Testing thermal gradient driving force for grain boundary migration using molecular dynamics simulations, *Acta Mater.* 85 (2015) 95–106, <https://doi.org/10.1016/j.actamat.2014.11.019>.
- [130] M.R. Tonks, Y. Zhang, A. Butterfield, X.-M. Bai, Development of a grain boundary pinning model that considers particle size distribution using the phase field method, *Model. Simulat. Mater. Sci. Eng.* 23 (2015), 045009, <https://doi.org/10.1088/0956-0393/23/4/045009>.
- [131] Y. Li, S. Hu, X. Sun, M. Stan, A review: applications of the phase field method in predicting microstructure and property evolution of irradiated nuclear materials, *Npj Comput. Mater.* 3 (2017) 1–16, <https://doi.org/10.1038/s41524-017-0018-y>.
- [132] R.N. Singh, Isothermal grain-growth kinetics in sintered  $\text{UO}_2$  pellets, *J. Nucl. Mater.* 64 (1977) 174–178, [https://doi.org/10.1016/0022-3115\(77\)90021-6](https://doi.org/10.1016/0022-3115(77)90021-6).
- [133] O.-V. Khoruzhii, S.-Y. Kourtchatov, V.-V. Likhanskii, New model of equiaxed grain growth in irradiated  $\text{UO}_2$ , *J. Nucl. Mater.* 265 (1999) 112–116, [https://doi.org/10.1016/S0022-3115\(98\)00632-1](https://doi.org/10.1016/S0022-3115(98)00632-1).
- [134] T. Wiss, V.V. Rondinella, R.J.M. Konings, D. Staicu, D. Papaioannou, S. Bremier, P. Pöml, O. Benes, J.-Y. Colle, P. Van Uffelen, A. Schubert, F. Cappia, M. Marchetti, D. Pizzocri, F. Jatuff, W. Goll, T. Sonoda, A. Sasahara, S. Kitajima, M. Kinoshita, Properties of the high burnup structure in nuclear light water reactor fuel, *Radiochim. Acta* 105 (2017) 893–906, <https://doi.org/10.1515/ract-2017-2831>.
- [135] D. Pizzocri, L. Luzzi, T. Barani, L. Cognini, A. Magni, A. Schubert, P. Van Uffelen, T. Wiss, Review of Available Models and Progress on the Sub-models Dealing with the Intra- and Intergranular Inert Gas Behaviour, 2019. <http://www.eera-jpnm.eu/inspyre/>.
- [136] J. Rest, G.L. Hofman, An alternative explanation for evidence that xenon depletion, pore formation, and grain subdivision begin at different local burnups, *J. Nucl. Mater.* 277 (2000) 231–238, [https://doi.org/10.1016/S0022-3115\(99\)00201-9](https://doi.org/10.1016/S0022-3115(99)00201-9).
- [137] P. Blair, A. Romano, C. Hellwig, R. Chawla, Calculations on fission gas behaviour in the high burnup structure, *J. Nucl. Mater.* 350 (2006) 232–239, <https://doi.org/10.1016/j.jnucmat.2006.01.006>.
- [138] M.S. Veshchunov, V.E. Shestak, Model for evolution of crystal defects in  $\text{UO}_2$  under irradiation up to high burn-ups, *J. Nucl. Mater.* 384 (2009) 12–18, <https://doi.org/10.1016/j.jnucmat.2008.09.024>.
- [139] M.S. Veshchunov, V.I. Tarasov, Modelling of pore coarsening in the high burn-up structure of  $\text{UO}_2$  fuel, *J. Nucl. Mater.* 488 (2017) 191–195, <https://doi.org/10.1016/j.jnucmat.2017.03.013>.
- [140] V.I. Tarasov, P.V. Polovnikov, V.E. Shestak, M.S. Veshchunov, Development of the MFPR/R code for characterization of the rim zone and high burnup structure evolution in  $\text{UO}_2$  fuel pellets, *J. Nucl. Mater.* 517 (2019) 214–224, <https://doi.org/10.1016/j.jnucmat.2019.01.055>.
- [141] M. Kinoshita, Mesoscopic approach to describe the high burn-up fuel behaviour, in: Enlarg. Halden Proj. Gr. Meet., Loen, Norway, 1999.